

1225-0767(ISSN Print)
2287-6715(ISSN Online)
한국연구재단 우수등재학술지

Journal of Ocean Engineering and Technology

Vol. 37, No. 2 (Serial Number 171)

April 2023

한국해양공학회지



www.joet.org



The Korean Society of Ocean Engineers

Editor-in-Chief

Choung, Joonmo Inha University, Korea

Editorial Board

Incecik, Atilla	University of Strathclyde, UK	Lee, Woo Dong	Gyeongsang National University, Korea
Jeong, Byongug	University of Strathclyde, UK	Li, Binbin	Tsinghua University, China
Jin, Chungkuk	Florida Institute of Technology, USA	Lim, Youngsub	Seoul National University, Korea
Kang, Hooi-Siang	Universiti Teknologi Malaysia, Malaysia	Oterkus, Erkan	University of Strathclyde, UK
Kim, Do Kyun	Seoul National University, Korea	Park, Hyoungsu	University of Hawaii at Manoa, USA
Kim, Jinwhan	Korea Advanced Institute of Science and Technology, Korea	Park, Jong Chun	Pusan National University, Korea
Kim, Kwon-Hoo	Pukyong National University, Korea	Shin, Sungwon	Hanyang University, Korea
Kim, Moo Hyun	Texas A&M University, USA	Srinil, Narakorn	Newcastle University, UK
Kim, Sang Jin	National Sun Yat-sen University, Taiwan	Tayyar, Gökhan Tansel	Istanbul Technical University, Türkiye
Kim, Taeseong	Technical University of Denmark, Denmark	Yu, Zhaolong	Norwegian University of Science and Technology, Norway
Koo, Weoncheol	Inha University, Korea		

Journal Publication Committee

Ahn, Seokhwan	Jungwon University, Korea	Kim, Seungjun	Korea University, Korea
Bae, Yoon Hyeok	Hongik University, Korea	Kim, Yeon-Joong	Korea Environment Institute, Korea
Cho, Gysung	Tongmyong University, Korea	Kim, Yeulwoo	Pukyong National University, Korea
Choi, Seongim	Gwangju Institute of Science and Technology, Korea	Kim, Younghun	Kyungnam University, Korea
Choi, Sung-Woong	Gyeongsang National University, Korea	Lee, Jooyong	Gyeongsang National University, Korea
Do, Kideok	Korea Maritime and Ocean University, Korea	Lee, Kangsu	Korea Research Institute of Ships & Ocean Engineering, Korea
Ham, Seung-Ho	Changwon National University, Korea	Lee, Tak Kee	Gyeongsang National University, Korea
Jeong, Se-Min	Chosun University, Korea	Nam, Bo Woo	Seoul National University, Korea
Jung, Dongho	Korea Research Institute of Ships & Ocean Engineering, Korea	Paik, Kwang-Jun	Inha University, Korea
Kang, Choonghyun	Gyeongsang National University, Korea	Seo, Jung Kwan	Pusan National University, Korea
Kang, TaeSoon	GeoSystem Research Corp., Korea	Song, Chang Yong	Mokpo National University, Korea
Kim, Hyun-Sik	Tongmyong University, Korea	Woo, Joohyun	Korea Maritime and Ocean University, Korea
Kim, Jeong-Hwan	Dong-A University, Korea	Yoon, Hyeon Kyu	Changwon National University, Korea

Research Ethics Committee

Kim, Jinwhan	Korea Advanced Institute of Science and Technology, Korea	Lee, Jin Ho	Pukyong National University, Korea
Kim, Joon-Young	Korea Maritime and Ocean University, Korea	Lee, Kangsu	Korea Research Institute of Ships & Ocean Engineering, Korea
Ko, Jae-Yong	Mokpo National Maritime University, Korea		

Published on April 30, 2023

Published by The Korean Society of Ocean Engineers (KSOE)
Room 1302, 13, Jungang-daero 180beon-gil, Dong-gu, Busan, 48821, Korea
TEL: +82-51-759-0656 FAX: +82-51-759-0657 E-mail: ksoehj@ksoe.or.kr URL: http://www.ksoe.or.kr

Printed by Hanrimwon Co., Ltd., Seoul, Korea E-mail: hanrim@hanrimwon.co.kr

ISSN(print) 1225-0767 ISSN(online) 2287-6715

This journal was supported by the Korean Federation of Science and Technology Societies (KOFST) grant funded by the Korean government.

© 2023 by The Korean Society of Ocean Engineers (KSOE)

This is an open access article distributed under the terms of the creative commons attribution non-commercial license (<http://creativecommons.org/licenses/by-nc/4.0>) which permits unrestricted non-commercial use, distribution, and reproduction in any medium, provided the original work is properly cited.

Journal of Ocean Engineering and Technology

한국해양공학회지

CONTENTS

Volume 37, Number 2

April, 2023

<Original Research Articles>

- Newton's Method to Determine Fourier Coefficients and Wave Properties for Deep Water Waves
JangRyong Shin 49
- Investigation of Applying Technical Measures for Improving Energy Efficiency Design Index (EEDI) for
KCS and KVLCC2
Jun-Yup Park, Jong-Yeon Jung and Yu-Taek Seo 58
- Field Observation and Quasi-3D Numerical Modeling of Coastal Hydrodynamic Response to Submerged Structures
Yejin Hwang, Kideok Do, Inho Kim and Sungyeol Chang 68

GENERAL INFORMATION

The “**Journal of Ocean Engineering and Technology**” (JOET) was launched in 1987 and is published bimonthly in February, April, June, August, October, and December each year by “The Korean Society of Ocean Engineers (KSOE).” Its ISO abbreviation is “J. Ocean Eng. Technol.” JOET publishes original research articles, technical articles, and review articles on all aspects of ocean engineering, including experimental, theoretical, numerical, and field observations. All manuscripts undergo peer-review by two or more reviewers.

The scope of JOET encompasses the following research areas:

- **Ships and offshore engineering:**

Design of ships and offshore structures; Resistance and propulsion; Seakeeping and maneuvering; Experimental and computational fluid dynamics; Ocean wave mechanics; Fatigue strength; Plasticity; Optimization and reliability; Arctic technology and extreme mechanics; Noise, vibration, and acoustics; Concrete engineering; Thermodynamics and heat transfer; Hydraulics and pneumatics; Autonomous and unmanned ship; Greenship technology; Digital twin of ships and offshore structures; Marine materials

- **Coastal engineering:**

Coastal, port, and harbor structures; Waves transformation; Coastal and estuary hydrodynamics; Sediment transport and morphological change; Subsea geotechnics; Coastal groundwater management; Prevention or mitigation of coastal disaster; Coastal zone development and management; Shore protection technique; Coastal environmental process; Beach safety

- **Ocean energy engineering:**


Offshore wind turbines; Wave energy platforms; Tidal current energy platforms; Floating photovoltaic energy platform; Small modular reactor; Combined energy platforms

- **Marine robot engineering:**

Robot sensor system; Autonomous navigation; Robot equipment; Marine robot control; Environment mapping and exploration; Underwater communication and networking; Design of marine robots

JOET is an open-access journal distributed under the terms of the creative commons attribution non-commercial license. It is indexed in databases such as the Korean Citation Index (KCI), Google Scholar, Science Central, Korea Science, and the Directory of Open Access Journals (DOAJ). JOET offers PDF or XML versions for free on its website (<https://www.joet.org>). For business matters, authors need to contact KSOE Secretariat by email or phone (e-mail: ksoehj@ksoe.or.kr or Tel: +82 51 759 0656). Correspondences for publication matters can be asked via email to the Editor-in-Chief (e-mail: heroeswise2@gmail.com).

Newton's Method to Determine Fourier Coefficients and Wave Properties for Deep Water Waves

JangRyong Shin ¹

¹Engineer, Offshore structure design department, Daewoo Shipbuilding & Marine Engineering co., LTD, Geoje, Korea

KEYWORDS: Fourier approximation, Stokes wave, Fenton's method, Deep-water breaking limit, Deep-water waves

ABSTRACT: Since Chappellear developed a Fourier approximation method, considerable research efforts have been made. On the other hand, Fourier approximations are unsuitable for deep water waves. The purpose of this study is to provide a Fourier approximation suitable even for deep water waves and a numerical method to determine the Fourier coefficients and the wave properties. In addition, the convergence of the solution was tested in terms of its order. This paper presents a velocity potential satisfying the Laplace equation and the bottom boundary condition (BBC) with a truncated Fourier series. Two wave profiles were derived by applying the potential to the kinematic free surface boundary condition (KFSBC) and the dynamic free surface boundary condition (DFSBC). A set of nonlinear equations was represented to determine the Fourier coefficients, which were derived so that the two profiles are identical at specified phases. The set of equations was solved using Newton's method. This study proved that there is a limit to the series order, i.e., the maximum series order is $N=12$, and that there is a height limitation of this method which is slightly lower than the Michell theory. The reason why the other Fourier approximations are not suitable for deep water waves is discussed.

1. Introduction

The undulations on the water surface adopt inherently beautiful forms, such as the smooth regular features of progressive waves. On the other hand, despite the innate curiosity concerning water wave motion, it was only in the 19th century by Airy that efforts to provide a mathematical description of wave motion began in earnest (Henry, 2008). Since the early development of the theory describing the waves using the perturbation method by Stokes (1847), many nonlinear solutions were obtained, both analytically and numerically.

Based on the use of truncated Fourier expansions for flow field quantities, Chappellear (1961) and Dean (1965) developed a 'Fourier approximation' (Tao et al., 2007). By choosing the expansions to satisfy the Laplace equation and the BBC, the problem was reduced to solving a set of nonlinear equations for each of the Fourier coefficients, and the wave properties (Tao et al., 2007). As the set of nonlinear equations is derived from the finite series, the expansions were represented by truncated Fourier expansions, which is why they are coined as Fourier approximations. Considerable research (Chappellear, 1961; Dean, 1965; Chaplin, 1979; Rienecker and Fenton, 1981; Fenton, 1988) has been conducted on this approach.

The stream function theory was developed by Dean (1965). Dean (1965) proposed the use of the root mean square errors (RMSE) in the dynamic free surface boundary condition (DFSBC) and the kinematic free surface boundary condition (KFSBC) as an error evaluation

criterion for wave theories. Dean (1965) also defined the Lagrangian function by introducing the linear summation of the two errors on the free surface with a Lagrange multiplier. Fourier coefficients were determined to minimize the Lagrangian function. The required order (N) of the stream function theory is determined by the wave steepness and shallow water parameter. For $N = 1$, the stream function theory reduces to the Airy wave theory. As the breaking wave height is approached, more terms are required to accurately represent the wave. Det Norske Veritas (DNV, 2010) described that stream function wave theory has an error of more than 1% in deep water waves whose height is over 90% of the breaking limit even though the required order is increased (See Figs. 3–4 in DNV (2010)). Chaplin (1979) applied the Schmidt orthogonalization process as an alternative to Dean's method and obtained improved results (Tao et al., 2007).

Rienecker and Fenton (1981) also adopted the stream function introduced by Dean (1965). The unknown constants were calculated directly with Newton's method in Rienecker and Fenton (1981). Therefore, the method required partial derivatives with regard to unknown constants, which complicated the numerical formulation of Newton's method. Fenton (1988) obtained all the partial derivatives for simplification of this method numerically. Because the reference depth parameter is simultaneously determined with the Fourier coefficients, the required order should be increased to reduce the numerical error in the water depth condition. Newton's method is unstable because the number of unknown coefficients increases when the required order

Received 17 November 2022, revised 2 February 2023, accepted 13 February 2023

Corresponding author JangRyong Shin: +82-55-735-5117, jrshin@dsme.co.kr

© 2023, The Korean Society of Ocean Engineers

This is an open-access article distributed under the terms of the creative commons attribution non-commercial license (<http://creativecommons.org/licenses/by-nc/4.0>) which permits unrestricted non-commercial use, distribution, and reproduction in any medium, provided the original work is properly cited.

increases. Therefore, the Newton method requires an initial solution closer to the exact solution. To solve it, in common with other versions of the Fourier approximation, it is sometimes necessary to solve a sequence of lower waves, extrapolating forward in height steps until the desired height is reached (Fenton, 1988). This problem can be avoided using the sequence of height steps (Fenton, 1990). As Rienecker and Fenton (1981) pointed out, several aspects of Fourier approximations beyond just the truncation of the series inhibited its widespread use (Tao et al., 2007). Neither of the above stream function approaches can be applied to waves in deep water because the stream function expansions contain hyperbolic functions (Fenton, 1988).

Shin (2016) reported that most numerical errors resulted from denominators in the stream function, the numerical integration of the water depth condition, and problems involved in Newton's method. Shin (2016) solved the problems by separately calculating the water depth condition and introducing deep water velocity potential without denominators and a dimensionless coordinate system. The flow field was represented with a velocity potential to satisfy the Laplace equation and the bottom boundary condition (BBC). Two wave profiles were calculated by applying the velocity potential to the KFSBC and the DFSBC. The potential contains $N+2$ unknown constants, which are N Fourier coefficients, the wave steepness, and the reference depth parameter, while the stream function contains $2N+6$ unknown constants (Rienecker and Fenton, 1981; Fenton, 1988). The wavelength and the reference depth parameter are not coupled to the Fourier coefficients because the dimensionless coordinate system was defined with the phase and the dimensionless elevation. Therefore, the wavelength and the reference depth parameter were determined independently. As a result, the required order was reduced in Shin (2016) and Shin (2021).

All the above-mentioned advantages resulted from the dimensionless coordinate system (Refer to Figs. 1 and 2). In addition to the advantages, there are some advantages to the coordinate system in Fig. 2. The independent variable is the relative horizontal position with regard to the wavelength in the moving coordinate system (Rienecker and Fenton, 1981; Fenton, 1988). The horizontal positions are also unknown values in Fenton's method because the wavelength is an unknown constant, which makes the numerical procedure much more complicated. On the other hand, the independent variable is the phase in the range $[0, \pi]$ in Shin (2016), which is a known value. In addition, partial derivatives with regard to the wavelength are unnecessary, unlike Fenton's method (Rienecker and Fenton, 1981; Fenton, 1988). All the partial derivatives necessary can be calculated with tensor analysis, while they are calculated numerically in Fenton's method. Therefore, there are no errors in the partial derivatives, unlike Fenton's method. The numerical formulation of Newton's method was also represented by tensor analysis.

Some waves near the breaking limit were calculated for verification, and their errors were checked with Dean's criteria. The deep water breaking limit was checked. According to the required order, the trend of numerical error was checked. There is a limit to the series order, i.e., $N \leq 12$. This is why the other approximations are unsuitable for deep water waves.

2. Complete Solution

The complete solution was presented by Shin (2016), and the results are summarized in this chapter. Two coordinate systems were adopted to describe a progressive water wave. One is the conventional coordinate

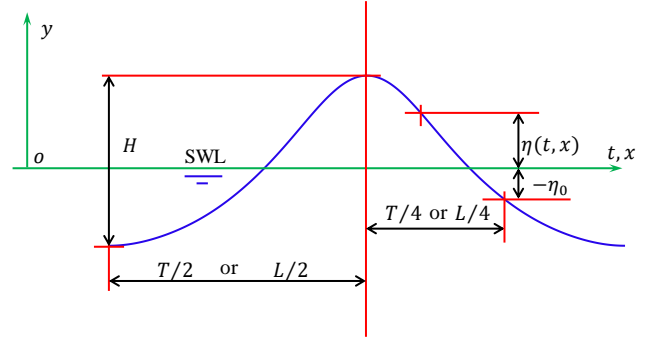


Fig. 1 Conventional coordinate system for a progressive wave (H : wave height, T : wave period, L : wavelength, $\eta(t, x)$: free surface elevation from the still water line (SWL)).

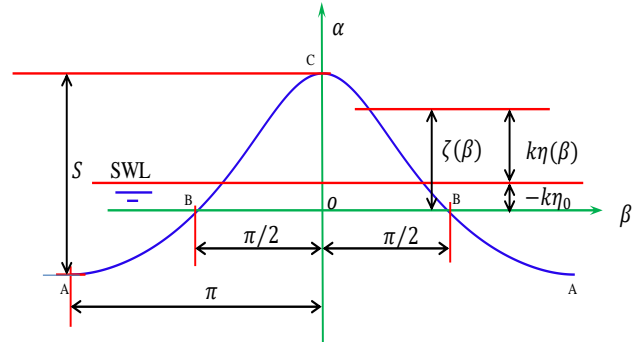


Fig. 2 Dimensionless coordinate system for a progressive wave.

system (t, x, y) shown in Fig. 1. The origin is located on the still water line. The x -axis is in the direction of the wave propagation, the y -axis points upwards, and t is time. The fluid domain is bounded by the free surface $y = \eta(t, x)$.

The other coordinate system (β, α) is the dimensionless stationary frame shown in Fig. 2. The origin is located at the point under the crest on the reference line, which is the horizontal line passing through two points at $\eta_o = \eta(\pm 90^\circ)$ on the free surface. Therefore, the wave profile is a fixed, periodic, and even function in the system. The horizontal axis is the phase, $\beta = kx - \omega t$, whose domain is $-\pi \leq \beta \leq \pi$, where k is the wave number defined by $k \triangleq 2\pi/L$ and ω is the angular frequency defined by $\omega \triangleq 2\pi/T$. The vertical axis is the dimensionless elevation from the reference line, $\alpha = k(y - \eta_o)$ in $\alpha \leq \zeta$, where $\zeta = k(\eta - \eta_o)$ is the dimensionless free surface elevation from the reference line.

The velocity potential in finite depth is represented in Shin (2019). The hyperbolic functions in the denominator are divergent as the water depth increases. Therefore, the potential is represented by the original deep water form without the hyperbolic functions.

$$\phi = \frac{\omega}{k^2} \sum_{n=1}^N a_n e^{n\alpha} \sin n\beta \quad (1)$$

where a_n is a Fourier coefficient, which is dimensionless. The horizontal water-particle velocity is

$$u(\beta, \alpha) = c \sum_{n=1}^N n a_n e^{n\alpha} \cos n\beta \quad (2)$$

where $c = \omega/k$ is the wave celerity. The vertical water-particle velocity is

$$v(\beta, \alpha) = c \sum_{n=1}^N n a_n e^{n\alpha} \sin n\beta \quad (3)$$

$\lim_{\alpha \rightarrow -\infty} v = 0$, which is the BBC. The water-particle accelerations in the horizontal direction and the vertical direction are represented as follows:

$$\frac{\partial u}{\partial t} = \frac{\omega^2}{k} \sum_{n=1}^N n^2 a_n e^{n\alpha} \sin n\beta \quad (4)$$

$$\frac{\partial v}{\partial t} = -\frac{\omega^2}{k} \sum_{n=1}^N n^2 a_n e^{n\alpha} \cos n\beta \quad (5)$$

The KFSBC is presented by an ordinary differential equation in the coordinate system. Solving the differential equation, the wave profile was calculated as follows (Refer to Appendix A):

$$\zeta = \sum_{n=1}^N a_n \left\{ e^{n\zeta} \cos n\beta - \cos \frac{n\pi}{2} \right\} \quad (6)$$

The integral constant was determined by the definition of the reference line, i.e., $\zeta(\pm\pi/2) = 0$. Eq. (6) contains only N coefficients, while Rienecker et al. (1981) contains $N+5$ unknown constants, which are $N+1$ coefficients, the wave number, celerity, volume rate, and Bernoulli's constant. Compared to Rienecker et al. (1981), Eq. (6) is simple. Unknown constants are reduced dramatically by introducing the coordinate system in Fig. 2. Bernoulli's equation is represented in the dimensionless coordinate system as follows:

$$\frac{p(\beta, \alpha)}{\rho c^2} = U(\beta, \alpha) - U_0 - \frac{1}{2} \{U^2(\beta, \alpha) + V^2(\beta, \alpha)\} + \frac{1}{2} (U_0^2 + V_0^2) - \frac{S\alpha}{\theta} \quad (7)$$

where ρ is the water density, and U and V are dimensionless horizontal and vertical velocities defined by $U \stackrel{\text{def}}{=} u/c$ and $V \stackrel{\text{def}}{=} v/c$. Bernoulli's constant is eliminated by the definition of the reference line, i.e., $p(\pm\pi/2, 0) = 0$. $U_0 = U(\pm\pi/2, 0)$ and $V_0 = V(\pm\pi/2, 0)$ are velocities at the phase of $\beta = \pm\pi/2$ on the free surface. The linear steepness is defined with $\theta \stackrel{\text{def}}{=} (\omega^2 H)/g$ where g is gravity and H is the wave height. The linear steepness is a constant for a particular wave. The other wave profile is calculated by applying the DFSBC ($p(\beta, \zeta) = 0$) to Eq. (7), as follows:

$$\frac{\zeta S}{\theta} = U(\beta, \zeta) - U_0 - \frac{1}{2} \{U^2(\beta, \zeta) + V^2(\beta, \zeta)\} + \frac{1}{2} (U_0^2 + V_0^2) \quad (8)$$

Eq. (8) contains only N coefficients and wave steepness. In addition, Eq. (8) also satisfies that $\zeta(\pm\pi/2) = 0$. Dimensionless wave height (steepness) is defined by $S \stackrel{\text{def}}{=} kH$, which provides the dispersion relation because the wave number is calculated as $k = S/H$. The reference line is determined by the water depth condition presented as follows:

$$k\eta_0 = -\frac{1}{2\pi} \int_{-\pi}^{\pi} \zeta d\beta \quad (9)$$

The steepness is determined by the wave height condition presented as follows:

$$S = \zeta(0) - \zeta(\pi) \quad (10)$$

For $N \rightarrow \infty$, Eqs. (1)–(10) provide the complete solution to irrotational deep water waves. The solution contains $N+2$ unknown constants, i.e., the Fourier coefficient, a_n , wave steepness, S , and reference depth parameter, $k\eta_0$.

This study aims to present a method to numerically determine the constants. $N+2$ equations are necessary to determine the unknown constants. The two profiles in Eqs. (6) and (8) should be identical for all phases. Hence, a set of N equations are obtained so that Eqs. (6) and (8) are equal at N phases. In addition, there are two equations, i.e., Eqs. (9) and (10). As a result, there are $N+2$ equations to determine the unknown constants.

An example for $N = 1$ and for $N = 2$ is presented in Appendix B and C, and Shin (2016) and Shin (2021) presented an example for $N = 3$. This method is further simplified and generalized by tensor analysis in the next chapter.

3. The Fourier Coefficients and the Steepness

A method to determine the Fourier coefficients and the steepness is presented for an arbitrary number of N .

In the other Fourier approximations (Rienecker and Fenton (1981), Fenton (1988)), the profile, η is directly calculated instead of ζ . Therefore, Eq. (9) must be simultaneously calculated with the coefficients. In this study, however, the profile η was calculated with ζ . Therefore, Eq. (9) was not coupled with the coefficients in this study and was calculated after they were determined. Hence, Eq. (9) is not considered in this chapter.

When the wave profile, ζ is prescribed in advance, it is possible to convert Eq. (6) to a set of linear equations to determine the coefficients. Because the wave profile is an even function, the phases β_m for $m = 1, 2, \dots, N$ are considered in the range, $0 \leq \beta_m \leq \pi$ and $\beta_m \neq \pi/2$ because Eqs. (6) and (8) already satisfy that $\zeta(\pm\pi/2) = 0$. $\beta_1 = 0$ and $\beta_N = \pi$. Letting $X_m = \zeta(\beta_m)$, Eq. (6) is represented at the phase β_m as follows:

$$K_{mn} a_n = X_m \quad (11)$$

The summation convention is considered in Eq. (11). The repeated subscript “ n ” is a dummy subscript. K_{mn} is a second-order tensor, a_n and X_m are vectors in N -dimensional space. The component of the tensor K_{mn} is presented as follows:

$$K_{mn} = e^{nX_m} \cos(n\beta_m) - \cos\left(\frac{n\pi}{2}\right) \quad (12)$$

Using the inverse tensor R_{mn} of the tensor K_{mn} , the solution to Eq. (11) is determined easily as follows:

$$a_n = R_{nm} X_m \quad (13)$$

Using Eq. (8), the error vector E_m in the DFSBC is defined as

$$E_m = -\frac{X_m S}{\theta} + U_{mn} a_n - \frac{1}{2} \varepsilon_{mpq} U_{pn} a_n \bar{U}_{qj} a_j - \frac{1}{2} \varepsilon_{mpq} V_{pn} a_n \bar{V}_{qj} a_j \quad (14)$$

where $S = X_1 - X_N$ from the wave height condition in Eq. (10).

Therefore, the wave height condition is automatically integrated in Eq. (14). The components of the second-order tensors in Eq. (14) are represented as follows:

$$U_{mn} = n \left\{ e^{nX_m} \cos(n\beta_m) - \cos\left(\frac{n\pi}{2}\right) \right\} \quad (15)$$

$$\bar{U}_{mn} = n \left\{ e^{nX_m} \cos(n\beta_m) + \cos\left(\frac{n\pi}{2}\right) \right\} \quad (16)$$

$$V_{mn} = n \left\{ e^{nX_m} \sin(n\beta_m) - \sin\left(\frac{n\pi}{2}\right) \right\} \quad (17)$$

$$\bar{V}_{mn} = n \left\{ e^{nX_m} \sin(n\beta_m) + \sin\left(\frac{n\pi}{2}\right) \right\} \quad (18)$$

The third-order tensor ε_{ijp} is defined as follows:

$$\varepsilon_{pqr} = \begin{cases} 1 & \text{for } p = q = r \\ 0 & \text{for the other case} \end{cases} \quad (19)$$

A set of N nonlinear equations represented by $E_m = 0$ for X_m are obtained by substituting Eq. (13) into Eq. (14). The set of equations is solved with Newton's method. A set of linear equations can be derived by denoting partial derivatives of a tensor using commas and indices as $\frac{\partial(\cdot)}{\partial X_i} = (\cdot)_{,i}$ and applying Newton's method to Eq. (14).

$$E_{m,i} \Delta X_i = -E_m \quad (20)$$

Because $\Delta X_i^{[r]} = X_i^{[r+1]} - X_i^{[r]}$, the solution in the next step is

$$X_i^{[r+1]} = X_i^{[r]} + \Delta X_i^{[r]} \quad (21)$$

The superscript $[r]$ with $[\]$ means the step of Newton's method. All the steps are r^{th} in all equations except Eq. (21) in this chapter. Therefore, for the simplification of equations, the superscript $[r]$ was omitted in all the equations except Eq. (21). Differentiating Eq. (14) with respect to X_i , the partial derivative $E_{m,i}$ of the error vector is

$$E_{m,i} = -\frac{\delta_{mi} S}{\theta} - \frac{X_m S_{,i}}{\theta} + U_{mn,i} a_n + U_{mn} a_{n,i} - \frac{1}{2} \varepsilon_{mpq} U_{pn,i} a_n \bar{U}_{qj} a_j - \frac{1}{2} \varepsilon_{mpq} U_{pn} a_{n,i} \bar{U}_{qj} a_j - \frac{1}{2} \varepsilon_{mpq} U_{pn} a_n \bar{U}_{qj,i} a_j - \frac{1}{2} \varepsilon_{mpq} U_{pn} a_n \bar{U}_{qj} a_{j,i} - \frac{1}{2} \varepsilon_{mpq} V_{pn,i} a_n \bar{V}_{qj} a_j - \frac{1}{2} \varepsilon_{mpq} V_{pn} a_{n,i} \bar{V}_{qj} a_j - \frac{1}{2} \varepsilon_{mpq} V_{pn} a_n \bar{V}_{qj,i} a_j - \frac{1}{2} \varepsilon_{mpq} V_{pn} a_n \bar{V}_{qj} a_{j,i} \quad (22)$$

Differentiating Eqs. (15)–(18) with respect to X_i , the components of the third-order tensors are

$$U_{mn,q} = \bar{U}_{mn,q} = n^2 \delta_{mq} e^{nX_m} \cos(n\beta_m) \quad (23)$$

$$V_{mn,q} = \bar{V}_{mn,q} = n^2 \delta_{mq} e^{nX_m} \sin(n\beta_m) \quad (24)$$

Because $S = X_1 - X_N$,

$$S_{,i} = \begin{cases} 1 & \text{for } i = 1 \\ 0 & \text{for } i \neq 1 \text{ or } N \\ -1 & \text{for } i = N \end{cases} \quad (25)$$

Differentiating Eq. (11) with respect to X_p , we have

$$K_{mn,p} a_n + K_{mn} a_{n,p} = \delta_{mp} \quad (26)$$

where $X_{m,p} = \delta_{mp}$ and δ_{mp} is the second-order isotropic tensor. Multiplying Eq. (26) by the tensor R_{im} , the partial derivative of the coefficient is easily determined as follows:

$$a_{i,p} = R_{ip} - R_{im} K_{mn,p} a_n \quad (27)$$

where $R_{im} K_{mn} = \delta_{in}$ and $\delta_{in} a_{n,p} = a_{i,p}$. Differentiating Eq. (12) with respect to X_p ,

$$K_{mn,p} = \delta_{mp} n e^{nX_m} \cos n\beta_m \quad (28)$$

Therefore, all the partial derivatives necessary were easily obtained without errors, unlike Fenton (1988).

Representing an individual component of a tensor as shown in Eqs. (12), (15)–(18), (23)–(24), and (28), the summation convention was not considered. As a criterion of convergence, the Root Mean Square Error in the DFSBC proposed by Dean (1965) was adopted. Dividing the inner product of the error vector E_m by N , the RMSE in the DFSBC (Dean, 1965) is defined as follows:

$$\text{RMSE} = \frac{\sqrt{E_m E_m}}{N} \times 100 \% \quad (29)$$

Newton's method was rapidly convergent to the complete solutions (whose RMSE $\leq 10^{-13}\%$ within three steps) when the result of Shin (2021) was used as the first step solution. There are some differences in the above approach compared to Fenton's method (Rienecker et al., 1981; Fenton, 1988).

- Eq. (11) is linear and decoupled from Eq. (20).
- All the partial derivatives with respect to wavelength are not required.
- All equations can be formulated with tensor analysis.
- X_i are merely parameters for calculating the coefficients and the steepness in this study. After determining the coefficients, X_i are no longer used. Hence, the wave elevation is denoted with X_i instead of ζ_i in Eqs. (11)–(28).
- After determining the coefficients and the steepness, the wave profile and water depth condition were calculated separately, as presented in the next chapter.

4. Wave Profile and Reference Depth Parameter

The Fourier coefficients and the steepness were determined in advance. Therefore, the wave profile can be calculated with Eq. (6) as follows: Eq. (6) is represented as

$$F(\beta, \zeta) = -\zeta + \sum_{n=1}^N a_n \left\{ e^{n\zeta} \cos n\beta - \cos \frac{n\pi}{2} \right\} \quad (30)$$

where $F(\beta, \zeta) = 0$. The power series of $F(\beta, \zeta)$ is represented as follows:

$$F(\beta, \zeta) = \sum_{q=0}^{\infty} \frac{F^{(q)}(\beta, 0)}{q!} \zeta^q \quad (31)$$

where $F^{(q)} = \frac{\partial^q F}{\partial \zeta^q}$. Because $F(\beta, \zeta) = 0$, Eq. (31) provides a polynomial equation with regard to ζ . For $q = 1$, Eq. (31) provides a linear equation. Eq. (31) provides a quadratic equation for $q = 2$, and Eq. (31) provides a cubic equation for $q = 3$. The equations provide good approximations to the wave profile because $|\zeta| < 1$ for all cases. For $q=2$, the following approximation is obtained:

$$\zeta^{[1]} = \frac{-F^{(1)}(\beta, 0) - \sqrt{\{F^{(1)}(\beta, 0)\}^2 - 2F(\beta, 0)F^{(2)}(\beta, 0)}}{F^{(2)}(\beta, 0)} \quad (32)$$

The other root is a trivial solution because it does not satisfy that $|\zeta| < 1$. The approximation is used as the first step in the Newton's method defined as follows. The superscript $[n]$ means the n^{th} step of Newton's method (where n is a natural number), while the superscript (n) means the n^{th} order partial derivative with respect to ζ . The wave profile is calculated as follows by applying Newton's method:

$$\zeta = \lim_{m \rightarrow \infty} \zeta^{[m+1]} \quad (33)$$

where

$$\zeta^{[m+1]} = \zeta^{[m]} - \frac{F(\beta, \zeta^{[m]})}{F'(\beta, \zeta^{[m]})} \quad (34)$$

$|F'(\beta, \zeta)| \geq |F'(0, \zeta_c)|$ for all waves and $|F'(0, \zeta_c)| = 0$ is the breaking condition proposed by Stokes (Chakrabarti, 1987). Therefore, Eq. (34) is valid for all waves except breaking waves. The Newton method rapidly converges to the complete solution. The wave elevations $\zeta_i = \zeta(\beta_i)$ were calculated using Eq. (33). Note that ζ_i stands for the free surface elevation at phase β_i . The integral is numerically calculated by substituting the results in water depth conditions as follows:

$$k\eta_0 = -\frac{1}{2M} \sum_{i=1}^M (\zeta_i + \zeta_{i+1}) \quad (35)$$

Because ζ is an even function, $\beta_1 = 0$, $\beta_i = (i-1)\pi/M$ and $\beta_{M+1} = \pi$. Note that M is independent of N . When M is increased, Eq. (35) can be calculated more accurately rather than Rienecker et al. (1981) and Fenton (1988).

5. Numerical Analysis Procedure

Fig. 3 presents a flow chart of the procedure. The chart comprises two DO-loops because the Fourier coefficients and wave profile are independently calculated. The first step, $X_m^{[1]}$, was calculated using the result in Shin (2021). The first DO-loop calculates the coefficients and the steepness. The coefficients, $a_n^{[r]}$ are calculated by Eq. (13). Substituting, $a_n^{[r]}$ into Eq. (20), $\Delta X_i^{[r]}$ are calculated by Eq. (20) and then $X_i^{[r+1]}$ are calculated by Eq. (21). The RMSE is calculated with Eq. (29). If the RMSE is greater than the tolerance ($1 \times 10^{-13}\%$), $X_i^{[r]}$ is replaced with $X_i^{[r+1]}$. The DO-loop continues until Newton's method converges to the complete solution within the tolerance.

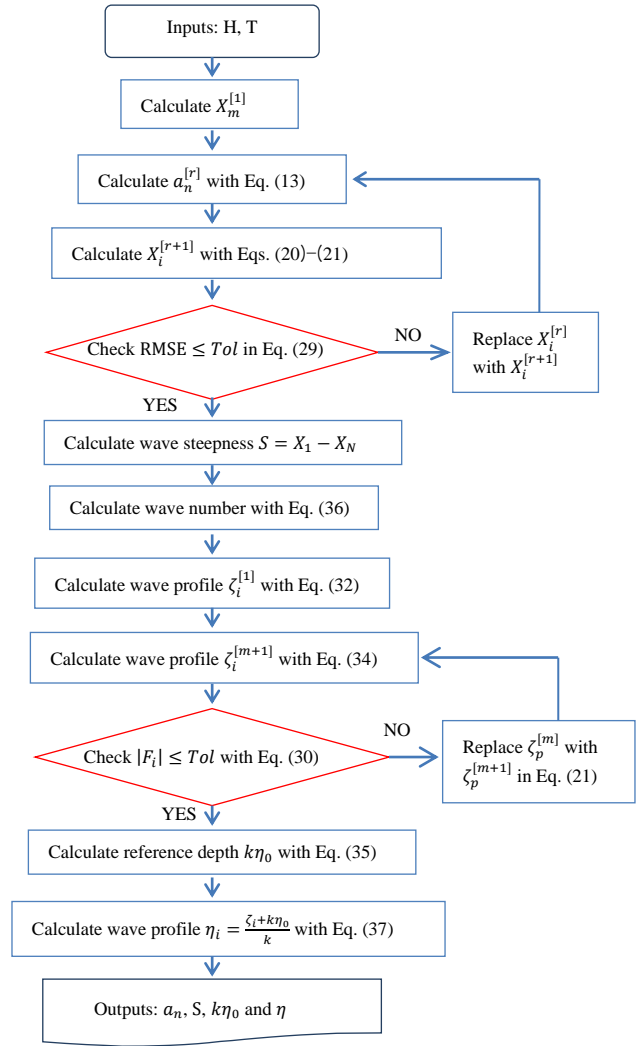


Fig. 3 Flow chart for numerical analysis.

In this DO-loop, the Fourier coefficients and the steepness are determined. The wave number is calculated as follows:

$$k = \frac{S}{H} \quad (36)$$

The second DO-loop is used to calculate the free surface elevations at more phases than the phases considered in the first DO-loop. The elevations, $\zeta_i^{[m+1]}$ are calculated using Newton's method in Eq. (34). The DO-loop continues until Newton's method converges to the complete solution within the tolerance ($|F(\beta_i, \zeta_i)| \leq 1 \times 10^{-17}$). Substituting ζ_i into Eq. (35), the reference depth parameter $k\eta_0$ was calculated. With the results, the wave profile was calculated as follows:

$$\eta_i = \frac{\zeta_i + k\eta_0}{k} \quad (37)$$

The water particle velocities were calculated by substituting the Fourier coefficients into Eqs. (2)–(3), and the accelerations were calculated by substituting the Fourier coefficients into Eqs. (4)–(5). The pressure field was calculated by substituting the Fourier coefficients into Eq. (7). The other wave profile was calculated by substituting the results into the right side of Eq. (8). The error in DFSBC can be checked by comparing the two profiles.

6. Results

The Fourier coefficients, a_n , the steepness, S , and the reference depth parameter, η_0 are functions of one variable whose independent variable is the linear steepness, θ . Consequently, Shin (2019) numerically calculated some data for the coefficients, steepness, and reference depth parameters in the range, $0 < \theta < 1$. By curve fitting the data, the Fourier coefficients, steepness, and reference depth parameter are represented by Newton's polynomials in Shin (2021), which give closed-form solutions. In this calculation, $N = 3$ was considered. The results satisfied the Laplace equation, the BBC, and the KFSBC. The RMSE in the DFSBC was less than 1% in the range, $H/L_o \leq 0.142$ where L_o is the linear wavelength defined as follows:

$$L_o = \frac{2\pi g}{\omega^2} \quad (38)$$

Because $\theta = 2\pi H/L_o$, $H/L_o = 0.142$ corresponds to $\theta = 0.892$. As a result, Shin (2016, 2021) reported a good approximation whose error was less than 1% in the range, $0 \leq \theta \leq 0.892$. Although the error increases, Shin (2021) still applies to the waves in the range, $0.892 \leq \theta < 0.999$. When $\theta > 0.999$, wave profile by Shin (2021) does not converge. Each researcher has a different criterion regarding deep water breaking limitations. Chakarabarti (1987) proposes $H/L_o = 0.142$. According to Dean and Dalrymple, (1984), Michell theory is $H/L_o = 0.17$, which corresponds to $H/L = 0.142$. According to Stokes, the breaking criterion is $u = c$ at the crest. In this study, the limitation was checked and the errors according to the required order were also checked. It is also discussed why the other Fourier approximations are unsuitable for deep water waves. For the verification, three waves with a period of 6 s are considered, which were tabulated in Table 1. The following series order was considered: $N = 1; N = 3, 6, 10, 12, 13$, and $35; M = 180$. The RMSE in the DFSBC was calculated and tabulated in Tables 2 and 3. As the required order is increased, the error is decreased. When $N \geq 13$, Newton's method in Ch. 3 did not converge because $e^{N\zeta}$ is very large and a_N is very small. As a result, this study is available for $N \leq 12$.

Eq. (35) was coupled with the other equations to calculate the Fourier coefficients, $N = M$ and Eq. (35) is calculated with $k\eta_0 = -\frac{1}{2N} \sum_{i=1}^N (X_i + X_{i+1})$ in Fenton's method. Therefore, the required order should be increased in Fenton's method. Because most errors of Fenton's method resulted from the numerical integration of the water depth condition, M should be increased to reduce it. Fenton's method, $M = N = 64$, is greater than $N=13$. Therefore, Fenton's method is unsuitable for deep water waves.

The wave height to wavelength ratio was calculated, as listed in Table 4. The wavelengths were similar to the 5th-order Stokes wave. When $\theta > 1.028$, this study does not converge. More precisely, Newton's method does not converge because the wave profile at the crest is sharp when $\theta > 1.028$. Therefore, $\theta = 1.028$ is the limitation of this study, which corresponds $H/L = 0.137$ and is slightly less than 0.142 according to Dean et al., (1984).

The convergent speed decreased when the required order increased. For $\theta \leq 0.892$, Shin (2021) is acceptable as the first step solution in Newton's method. For $\theta > 0.892$, the method reported by Shin (2021) is unsuitable for the first step solution because the Newton method does not converge. This problem can be avoided using the sequence of height steps. For waves in the range $0.892 < \theta \leq 0.999$, the profile

for $\theta = 0.892$ is used as the first step solution, and for waves in the range $0.999 < \theta \leq 1.028$, the profile for $\theta = 0.999$ is used as the first step solution. The profiles are shown in Fig. 4; the horizontal velocities are shown in Fig. 5; the vertical velocities are shown in Fig. 6. The relative horizontal velocity at the crest is 0.782 for wave (c), which is less than Stokes' criteria, 1. The Bernoulli's constant in Fig. 4 is calculated for wave (c).

Table 1 Test waves with period $T = 6$ s

	Wave (a)	Wave (b)	Wave (c)
θ	0.892	0.999	1.028
H (m)	7.980	8.937	9.196
H/L_o	0.142	0.159	0.164

Table 2 RMSE (%)

Theories	$\theta = 0.892$	$\theta = 0.999$	$\theta = 1.028$
5 th Stokes	2.492	3.950	4.459
$N = 1$	1.758	2.226	2.360
Shin (2021)	8.26E-2	1.13	Not applicable
$N = 6$	1.08E-2	9.38E-2	2.15E-1
$N = 10$	2.78E-4	8.21E-3	2.94E-2
$N = 12$	6.05E-5	4.85E-3	2.04E-2

Table 3 RMSE (%) as per Newton's method step for $N = 12$

Wave	(a)	(b)	(c)
Step 1	0.207	2.34 ¹⁾	0.628 ¹⁾
Step 2	3.27E-3	0.285	3.15E-2
Step 3	6.06E-5	2.01E-2	2.04E-2 ²⁾
Step 4	6.05E-5	4.85E-3	2.55E-2 ²⁾

Note that $1\text{En} = 1 \times 10^{\text{th}}$.

¹⁾ Note that 0.628% is less than 0.207% or 2.34%. The reason is that the first step for wave (c) is the wave profile of wave (b) in step 4, and the first step for wave (b) is the wave profile of wave (a) in step 4, while the first step for wave (a) is the result by Shin (2021) with $N = 3$.

²⁾ Note that 2.55E-2 is greater than 2.04E-2. It means that the minimum error is 2.04E-2. As the step is increased, the error oscillates between the two values.

Table 4 Wave height to wavelength ratio, H/L .

Theories	$\theta = 0.892$	$\theta = 0.999$	$\theta = 1.028$
Airy	0.142	0.159	0.164
5 th Stokes	0.123	0.135	0.138
$N = 1$	0.119	0.129	0.131
Shin (2021)	0.123	0.135	Not applicable
$N = 6$	0.123	0.134	0.137
$N = 10$	0.123	0.134	0.137
$N = 12$	0.123	0.134	0.137

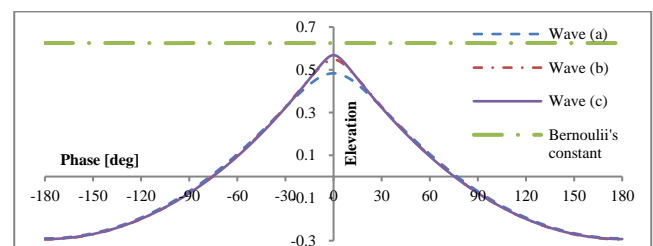


Fig. 4 Dimensionless wave profiles calculated with $N = 12$ (ordinate is the dimensionless elevation from the still water line (SWL), $k\eta$)

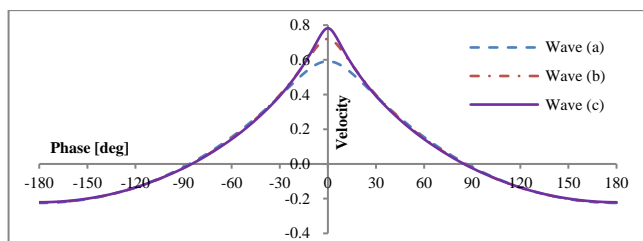


Fig. 5 Relative horizontal velocities calculated with $N = 12$ (the ordinate is the dimensionless velocity, u/c)

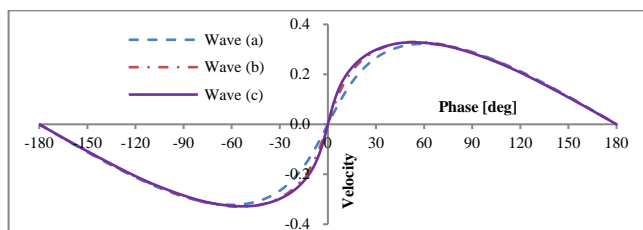


Fig. 6 Relative vertical velocities calculated with $N = 12$ (the ordinate is the dimensionless velocity, v/c)

7. Conclusions

This study aimed to provide a numerical method to calculate the Fourier coefficient, steepness, and reference depth parameter. The numerical procedure is much more simplified than Fenton's method (Rienecker et al., 1981). The major simplifications are as follows:

(1) Although the moving coordinate system by Dean was adopted in Fenton's method, a dimensionless coordinated system was adopted in this study. As a result, all the partial derivatives with respect to wavelength are not required. Some parameters were eliminated.

(2) All equations were formulated by tensor analysis. Therefore, numerical equations were much more simplified and had no errors.

(3) In the other Fourier approximation, the required order was determined to reduce the error of the numerical integration in the water depth condition because it was solved simultaneously with the Fourier coefficients. On the other hand, the water depth condition was calculated independently. Therefore, the required order was reduced dramatically.

The error was reduced when the required order was increased. Nevertheless, there is a limit to the required order. This study is not applicable when $N \geq 13$. Deep water breaking limitation was checked. This study is valid for waves in the range, $0 < \theta \leq 1.028$. The limitation 1.028 correspond to $H/L = 0.137$, which is slightly lower than the Michell theory.

Conflict of Interest

The authors declare that they have no conflict of interest.

References

Chakrabarti, S. K. (1987). *Hydrodynamics of Offshore structures*. London, UK: Computational Mechanics Publications.
 Chaplin, J. R. (1979). Developments of stream-function wave theory. *Journal of Coastal Engineering*, 3, 179–205. [https://doi.org/10.1016/0378-3839\(79\)90020-6](https://doi.org/10.1016/0378-3839(79)90020-6)

Chappelear, J. E. (1961). Direct numerical calculation of wave properties. *Journal of Geophysical Research*, 66(2), 501–508. <https://doi.org/10.1029/JZ066i002p00501>
 Dean, R. G. (1965). Stream function representation of nonlinear ocean waves. *Journal of Geophysical Research*, 70(18), 4561–4572. <https://doi.org/10.1029/JZ070i018p04561>
 Dean, R. G. & Dalrymple, R. A. (1984). *Water wave mechanics for engineers and scientists*. Prentice-Hall, Inc.
 Det Norske Veritas (DNV). (2010). Environmental conditions and environmental loads. *Recommended Practice DNV-RP-C205*.
 Fenton, J. D. (1988). The numerical solution of steady water wave problems. *Computers & Geosciences*, 14(3), 357–368. [https://doi.org/10.1016/0098-3004\(88\)90066-0](https://doi.org/10.1016/0098-3004(88)90066-0)
 Fenton, J. D. (1990). Nonlinear wave theories. In B. Le Méhauté, D.M. Hanes (Eds.), *Ocean Engineering Science, The Sea*, 9, Wiley.
 Rienecker, M. M., & Fenton, J. D. (1981). A Fourier Approximation Method for Steady Water Waves. *Journal of Fluid Mechanics*, 104, 119–137. <https://doi.org/10.1017/S0022112081002851>
 Shin, J. (2016). Analytical Approximation in Deep Water Waves. *Journal of Advanced Research in Ocean Engineering*, 2(1), 1–11. <https://doi.org/10.5574/JAROE.2016.2.1.001>
 Shin, J. (2019). A Regression Analysis Result for Water Waves on Irrotational Flow over a Horizontal Bed. *International Journal of Offshore Polar Engineering. IJOPE*, 29(4), 461–466. <https://doi.org/10.17736/ijope.2019.hc17>
 Shin, J. (2021). A Fourier series approximation for deep-water waves. *Journal of Ocean Engineering and Technology*, 36(2), 101–107. <https://doi.org/10.26748/KSOE.2021.092>
 Stokes, G. G. (1847). On the Theory of Oscillatory Waves. *Transactions of the Cambridge Philosophical Society*, 8, 441–473.
 Tao, L., Song, H., & Chakrabarti, S. (2007). Nonlinear progressive waves in water of finite depth -an analytic approximation. *Coastal Eng.*, 54(11), 825–834.

Author ORCID

Author name	ORCID
Shin, JangRyong	0000-0002-0144-2084

Appendices

Appendix A. Solution to KFSBC

The KFSBC is presented in the conventional coordinate system as follows:

$$v = \frac{\partial \eta}{\partial t} + u \frac{\partial \eta}{\partial x} \quad (A1)$$

Because $\zeta = k(\eta - \eta_0)$, we have

$$\frac{\partial \eta}{\partial t} = -\omega \frac{\partial}{\partial \beta} \left\{ \frac{\zeta}{k} + \eta_0 \right\} = -\frac{\omega}{k} \frac{\partial \zeta}{\partial \beta} = -c \frac{\partial \zeta}{\partial \beta} = -c \frac{d\zeta}{d\beta} \quad (A2)$$

As $\zeta = \zeta(\beta)$, then we have

$$\frac{\partial \zeta}{\partial \beta} = \frac{d\zeta}{d\beta} \quad (\text{A3})$$

And

$$\frac{\partial \eta}{\partial x} = k \frac{\partial}{\partial \beta} \left\{ \frac{\zeta}{k} + \eta_0 \right\} = \frac{\partial \zeta}{\partial \beta} = \frac{d\zeta}{d\beta} \quad (\text{A4})$$

Substituting Eqs. (A2) and (A4) into Eq. (A1), the KFSBC is presented in the dimensionless coordinate system as follows:

$$v = -c \frac{d\zeta}{d\beta} + u \frac{d\zeta}{d\beta} \quad (\text{A5})$$

Substituting Eqs. (2) and (3) into Eq. (A5),

$$c \sum_{n=1}^N n a_n e^{n\zeta} \sin n\beta = -c \frac{d\zeta}{d\beta} + \left\{ c \sum_{n=1}^N n a_n e^{n\zeta} \cos n\beta \right\} \frac{d\zeta}{d\beta} \quad (\text{A6})$$

Because $\alpha = \zeta$ on the free surface, then the water particle velocities are presented as follows:

$$u(\beta, \zeta) = c \sum_{n=1}^N n a_n e^{n\zeta} \cos n\beta \quad (\text{A7})$$

and

$$v(\beta, \zeta) = c \sum_{n=1}^N n a_n e^{n\zeta} \sin n\beta \quad (\text{A8})$$

Dividing Eq. (A6) by the celerity and multiplying the result by $d\beta$,

$$\left\{ \sum_{n=1}^N n a_n e^{n\zeta} \sin n\beta \right\} d\beta = -d\zeta + \left\{ \sum_{n=1}^N n a_n e^{n\zeta} \cos n\beta \right\} d\zeta \quad (\text{A9})$$

The above is presented as follows

$$d\zeta = \left\{ \sum_{n=1}^N n a_n e^{n\zeta} \cos n\beta \right\} d\zeta - \left\{ \sum_{n=1}^N n a_n e^{n\zeta} \sin n\beta \right\} d\beta \quad (\text{A10})$$

Where the first term on the right-hand side of Eq. (A10) is presented as follows:

$$\left\{ \sum_{n=1}^N n a_n e^{n\zeta} \cos n\beta \right\} d\zeta = \frac{\partial}{\partial \zeta} \left\{ \sum_{n=1}^N a_n e^{n\zeta} \cos n\beta \right\} d\zeta \quad (\text{A11})$$

The second term on the right-hand side of Eq. (A10) is presented as follows:

$$-\left\{ \sum_{n=1}^N n a_n e^{n\zeta} \sin n\beta \right\} d\beta = \frac{\partial}{\partial \beta} \left\{ \sum_{n=1}^N a_n e^{n\zeta} \cos n\beta \right\} d\beta \quad (\text{A12})$$

The right-hand-side of Eq. (A10) is presented as follows:

$$d\zeta = d \left\{ \sum_{n=1}^N a_n e^{n\zeta} \cos n\beta \right\} \quad (\text{A13})$$

Integrating the above equation,

$$\zeta = \sum_{n=1}^N a_n e^{n\zeta} \cos n\beta + C_1 \quad (\text{A14})$$

Using the definition of the reference line (Refer to Fig. 2), we have $\zeta \left(\pm \frac{\pi}{2} \right) = 0$, then the integral constant is determined as follows:

$$C_1 = - \sum_{n=1}^N a_n \cos \frac{n\pi}{2} \quad (\text{A15})$$

Substituting Eq. (A15) into Eq. (A14) results in Eq. (6).

Appendix B. Solution for N=1

For $N = 1$, the wave profile in Eq. (6) is represented as follows:

$$\zeta = a_1 e^{\zeta} \cos \beta \quad (\text{A16})$$

From Eq. (8), the other wave profile is represented as follows:

$$\frac{\zeta S}{\theta} = a_1 e^{\zeta} \cos \beta - \frac{a_1^2 e^{2\zeta}}{2} + \frac{a_1^2}{2} \quad (\text{A17})$$

From Eq. (A16), crest height, i.e., the elevation at $\beta = 0$ is determined as follows:

$$\zeta_c = a_1 e^{\zeta_c} \quad (\text{A18})$$

Therefore, the Fourier coefficient is determined as follows:

$$a_1 = \zeta_c e^{-\zeta_c} \quad (\text{A19})$$

From Eq. (A16), trough depth, i.e., the elevation at $\beta = \pi$ is determined as follows:

$$\zeta_t = -a_1 e^{\zeta_t} \quad (\text{A20})$$

By substituting Eq. (A19) into Eq. (A20) and substituting Eq. (10) into the result, $\zeta_t = -\zeta_c e^{-S}$. Substituting it into Eq. (10) allows the crest height to be determined as follows:

$$\zeta_c = \frac{S}{1 + e^{-S}} \quad (\text{A21})$$

The trough depth is determined by substituting Eq. (A21) into $\zeta_t = -\zeta_c e^{-S}$:

$$\zeta_t = -\frac{S e^{-S}}{1 + e^{-S}} \quad (\text{A22})$$

The wave steepness is determined so that Eq. (A16) and Eq. (A17) meet at phase $\beta = 0$. Therefore the following equation can be used:

$$\frac{S}{1 - \frac{S}{2(1 + e^{-S})} \left\{ 1 - \exp \left(\frac{-2S}{1 + e^{-S}} \right) \right\}} = \theta \quad (\text{A23})$$

Eq. (A23) is the dispersion relation. For small amplitude, an approximation to Eq. (A23) is $S = \theta$, which gives the linear dispersion relation $\omega^2 = gk$. Applying Newton's method to Eq. (A23), the steepness was calculated as follows

$$S = \lim_{m \rightarrow \infty} S^{[m+1]} \quad (\text{A24})$$

Where $S^{[1]} = \theta$ and

$$S^{[m+1]} = S^{[m]} - \frac{f(S^{[m]})}{f'(S^{[m]})} \quad (\text{A25})$$

From Eq. (A23),

$$f(S) = 2S(1 + e^{-S}) - \theta \left[2(1 + e^{-S}) - \exp\left(-\frac{2S}{1 + e^{-S}}\right) \right] \quad (\text{A26})$$

And differentiating Eq. (A26) with regard to S ,

$$f'(S) = 2(1 + e^{-S}) - 2Se^{-S} - \theta \left[-2e^{-S} - \left\{ 1 - \exp\left(-\frac{2S}{1 + e^{-S}}\right) \right\} - 2 \left\{ \frac{1 + e^{-S} + Se^{-S}}{(1 + e^{-S})^2} \right\} \exp\left(-\frac{2S}{1 + e^{-S}}\right) \right] \quad (\text{A27})$$

The wave profile is calculated with the method in Ch. 3, in which $F(\beta, \zeta) = -\zeta + a_1 e^\zeta \cos \beta$. This result has an error of less than 1.165% for waves in the range, $H/L_o \leq 0.142$, which is less than the error of the 5th order Stokes' wave theory. Wave (c) was calculated with $N = 1$, $N = 12$, and the 5th Stokes theory, and the results were compared in Figs. A1–A3. $N = 1$ gave similar results as the 5th Stokes theory. Comparing Fig. 4 and Fig. A1, the wave profiles calculated by $N = 1$, and the 5th Stokes theory was less sharp than those calculated by $N = 12$.

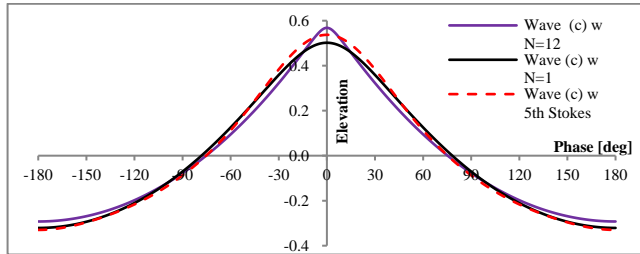


Fig. A1 Dimensionless wave profiles calculated with $N = 1$, $N = 12$, and 5th Stokes theory (the ordinate is the dimensionless elevation from SWL, $k\eta$)

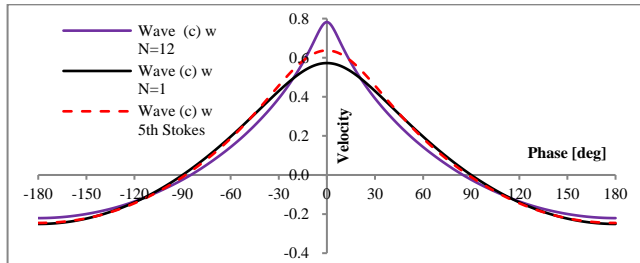


Fig. A2 Relative horizontal velocities calculated with $N = 1$, $N = 12$, and 5th Stokes theory (the ordinate is the dimensionless velocity, u/c)

Appendix C. Solution for $N=2$

For $N=2$, Eq. (6) is represented as follows:

$$\zeta = a_1 e^\zeta \cos \beta + a_2 e^{2\zeta} \cos 2\beta + a_2 \quad (\text{A28})$$

Eq. (8) is represented as follows:

$$\frac{\zeta S}{\theta} = a_1 e^\zeta \cos \beta + 2a_2 e^{2\zeta} \cos 2\beta - \frac{a_1^2 e^{2\zeta}}{2} - 2a_2^2 e^{2\zeta} - 2a_1 a_2 e^{3\zeta} \cos \beta + 2a_2 + \frac{a_1^2}{2} + 2a_2^2 \quad (\text{A29})$$

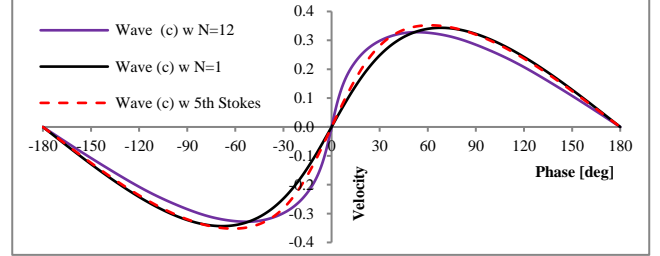


Fig. A3 Relative vertical velocities calculated with $N = 1$, $N = 12$, and 5th Stokes theory (the ordinate is the dimensionless velocity, v/c)

The coefficients are determined so that Eqs. (A28) and (A29) are equal to each other at phase $\beta = 0$ and $\beta = \pm\pi$ and to satisfy Eq. (10). Eq. (A28) is represented for $X_1 = \zeta(0)$ as follows:

$$X_1 = a_1 e^{X_1} + a_2 (e^{2X_1} + 1) \quad (\text{A30})$$

Eq. (A28) is represented for $X_2 = \zeta(\pi)$ as follows:

$$X_2 = -a_1 e^{X_2} + a_2 (e^{2X_2} + 1) \quad (\text{A31})$$

Solving Eqs. (A30)–(A31) for a_1 and a_2 , the two coefficients are determined as follows:

$$a_1 = \frac{X_1 (e^{2X_2} + 1) - X_2 (e^{2X_1} + 1)}{e^{X_1} (e^{2X_2} + 1) + e^{X_2} (e^{2X_1} + 1)} \quad (\text{A32})$$

and

$$a_2 = \frac{X_2 e^{X_1} + X_1 e^{X_2}}{e^{X_1} (e^{2X_2} + 1) + e^{X_2} (e^{2X_1} + 1)} \quad (\text{A33})$$

The error of Eq. (A29) for $X_1 = \zeta(\pi)$ is represented as follows:

$$E_1 = -\frac{X_1 (X_1 - X_2)}{\theta} + a_1 e^{X_1} + 2a_2 e^{2X_1} - \frac{a_1^2 e^{2X_1}}{2} - 2a_2^2 e^{2X_1} - 2a_1 a_2 e^{3X_1} + 2a_2 + \frac{a_1^2}{2} + 2a_2^2 \quad (\text{A34})$$

The error of Eq. (A29) is represented for $X_2 = \zeta(\pi)$ as follows:

$$E_2 = -\frac{X_2 (X_1 - X_2)}{\theta} - a_1 e^{X_2} + 2a_2 e^{2X_2} - \frac{a_1^2 e^{2X_2}}{2} - 2a_2^2 e^{2X_2} + 2a_1 a_2 e^{3X_2} + 2a_2 + \frac{a_1^2}{2} + 2a_2^2 \quad (\text{A35})$$

Therefore, there are five equations, i.e., Eqs. (A32)–(A35) and Eq. (10) to determine the unknown constants, a_1 , a_2 , X_1 , X_2 , and S . The set of equations was solved with Newton's method presented in Ch. 3. The reference depth parameter and wave profile were determined using the method presented in Ch. 4.

Investigation of Applying Technical Measures for Improving Energy Efficiency Design Index (EEDI) for KCS and KVLCC2

Jun-Yup Park¹, Jong-Yeon Jung¹ and Yu-Taek Seo²

¹Graduate student, Department of Naval Architecture and Ocean Engineering, Seoul National University, Seoul, Korea

²Professor, Department of Naval Architecture and Ocean Engineering, Seoul National University, Seoul, Korea

KEYWORDS: Energy efficiency design index, Energy saving device, On-board carbon capture and storage

ABSTRACT: While extensive research is being conducted to reduce greenhouse gases in industrial fields, the International Maritime Organization (IMO) has implemented regulations to actively reduce CO₂ emissions from ships, such as energy efficiency design index (EEDI), energy efficiency existing ship index (EEXI), energy efficiency operational indicator (EEOI), and carbon intensity indicator (CII). These regulations play an important role for the design and operation of ships. However, the calculation of the index and indicator might be complex depending on the types and size of the ship. Here, to calculate the EEDI of two target vessels, first, the ships were set as Deadweight (DWT) 50K container and 300K very large crude-oil carrier (VLCC) considering the type and size of those ships along with the engine types and power. Equations and parameters from the marine pollution treaty (MARPOL) Annex VI, IMO marine environment protection committee (MEPC) resolution were used to estimate the EEDI and their changes. Technical measures were subsequently applied to satisfy the IMO regulations, such as reducing speed, energy saving devices (ESD), and onboard CO₂ capture system. Process simulation model using Aspen Plus v10 was developed for the onboard CO₂ capture system. The obtained results suggested that the fuel change from Marine diesel oil (MDO) to liquefied natural gas (LNG) was the most effective way to reduce EEDI, considering the limited supply of the alternative clean fuels. Decreasing ship speed was the next effective option to meet the regulation until Phase 4. In case of container, the attained EEDI while converting fuel from Diesel oil (DO) to LNG was reduced by 27.35%. With speed reduction, the EEDI was improved by 21.76% of the EEDI based on DO. Pertaining to VLCC, 27.31% and 22.10% improvements were observed, which were comparable to those for the container. However, for both vessels, additional measure is required to meet Phase 5, demanding the reduction of 70%. Therefore, onboard CO₂ capture system was designed for both KCS (Korea Research Institute of Ships & Ocean Engineering (KRISO) container ship) and KVLCC2 (KRISO VLCC) to meet the Phase 5 standard in the process simulation. The absorber column was designed with a diameter of 1.2-3.5 m and height of 11.3 m. The stripper column was 0.6-1.5 m in diameter and 8.8-9.6 m in height. The obtained results suggested that a combination of ESD, speed reduction, and fuel change was effective for reducing the EEDI; and onboard CO₂ capture system may be required for Phase 5.

1. Introduction

Global warming has caused many problems worldwide. To address such problems, eco-friendly decarbonization regulations have been implemented. In the ship market, the International Maritime Organization (IMO), which oversees maritime affairs around the world, has also enacted related regulations. For newly built ships from 2013, the energy efficiency design index (EEDI), which indicates carbon dioxide emissions for transporting one ton of cargo over one nautical mile, must conform with the regulations. To this end, designing ships with high energy efficiency right from the design stage is necessary. Since the amount to be reduced increases for each phase, research has been actively conducted to improve the hull form and

propulsion systems (KIOST, 2016).

To improve the index, a remodeling method of the propulsion system that uses liquefied natural gas (LNG) rather than low-sulfur fuel oil or conventional bunker fuels is required. Jung (2014), Jung et al. (2022), and marine environment protection committee (MEPC) 79/7/4 (IMO, 2022) proposed a method of installing an onboard carbon capture and storage (OCCS) system in ships, to capture CO₂ emitted from ships.

Methods to reduce resistance by remodeling the bow shape and improve the propulsion efficiency by installing energy saving devices (ESDs) before and after the stern propeller are also available. In general, ESD installation increases the propulsion efficiency by 5% on average based on the transmission power. Song et al. (2015) applied a

Received 9 January 2023, revised 20 February 2023, accepted 28 March 2023

Corresponding author Yutaek Seo: +82-2-880-7329, yutaek.seo@snu.ac.kr

© 2023, The Korean Society of Ocean Engineers

This is an open access article distributed under the terms of the creative commons attribution non-commercial license (<http://creativecommons.org/licenses/by-nc/4.0>) which permits unrestricted non-commercial use, distribution, and reproduction in any medium, provided the original work is properly cited.

system that generates an acceleration effect using a duct and improves propulsion by recovering the kinetic energy lost in the wake of the propeller using a pre-swirl stator to a 176K bulk carrier. Kim et al. (2015) conducted computational fluid dynamics (CFD) analysis and model tests by attaching the developed pre-swirl stator and duct-combined pre-swirl stator to the 317K very large crude oil carrier (VLCC) hull form. They found that the transmission power was reduced by 3% for the pre-swirl stator and 6.1% for the duct-combined pre-swirl stator. Park and Cho (2017) modified the bulbous bow to ensure suitability for the slow steaming of an 8,600 TEU container ship and applied the operational efficiency index calculation formula modified based on a comparison of fuel consumption before and after the modification. They derived the index reduction rate and carbon dioxide reduction before and after the modification, according to the supercharger operating conditions at 14 to 20 knots (25.93 to 37.04 km/h). Choi and Rho (2011) mentioned the limitations of the fuel consumption rate calculation method for cargo volume in determining the energy efficiency operational indicator (EEOI) of IMO and presented an improved calculation formula for the indicator that applies the fuel consumption per kW related to the engine load. They also calculated and analyzed carbon dioxide emissions by applying actual ship operation data to the improved calculation formula. Shin et al. (2013) conducted research on the design, numerical analysis, and evaluation methods related to the ESD development procedure for a 73K tanker. They confirmed the fuel-saving effect of 4–6% when the developed ESD was applied to various low-speed and large full form ship.

Application of various technical and operational measures for satisfying the environmental regulations presented by IMO is necessary. Thus far, various technical measures have been proposed,

including ship speed reduction, hull form improvement, low-friction paint utilization, wind power propulsion, air lubrication system, waste heat recovery system, and OCCS. Along with these, certain operational measures, such as route optimization, operating speed optimization, trim optimization, optimal fleet management, port loading/unloading optimization, and shore to ship (S2S), have also been considered. Here, ships that correspond to KCS (Korea Research Institute of Ships & Ocean Engineering (KRISO) container ship) and KVLCC2 (KRISO VLCC) types were set as target vessels, and an attempt was made to examine improved EEDI and IMO regulations under the application of technical measures, such as speed reduction, ESD installation, and OCCS. To this end, the EEDI calculation formula presented by IMO was used. For the efficiency improvement effect by ESD, the values in the literature were applied. In the case of OCCS, a system of the required size was designed through process simulation. It is expected to prove the effect by means of mandatory CO₂ reduction in ships and the justification for OCCS, making research in the related field more active.

2. EEDI Calculation for KCS and KVLCC2

2.1 Calculation Method

The contents of MEPC.203(62) (IMO, 2011), MEPC.245(66) (IMO, 2014), and MEPC.308(73) (IMO, 2018) were referred to for contents related to EEDI calculation. Whether this index satisfies IMO regulations can be confirmed by obtaining and comparing the Attained EEDI, Reference line, and Required EEDI values. Attained EEDI is the value calculated using Eq. (1) below. Reference line is a reference value for calculating the required EEDI for each ship type. The required EEDI can be obtained by substituting the reduction factor (X)

Table 1 X values of each phase for the required EEDI calculation (DWT, Deadweight) (IMO, 2011)

Type	Size (DWT)	Phase 0 (2013.01.01. –2014.12.31)	Phase 1 (2015.01.01. –2019.12.31.)	Phase 2 (2020.01.01. –2024.12.31.)	Phase 3 (2025.01.01.–)	Phase 4	Phase 5
Bulk carrier	20,000 and above	0	10	20	30		
	10,000–20,000	n/a	0–10 ¹⁾	0–20 ¹⁾	0–30 ¹⁾		
Gas carrier	10,000 and above	0	10	20	30		
	2,000–10,000	n/a	0–10 ¹⁾	0–20 ¹⁾	0–30 ¹⁾		
Tanker	20,000 and above	0	10	20	30		
	4,000–20,000	n/a	0–10 ¹⁾	0–20 ¹⁾	0–30 ¹⁾		
Container ship	15,000 and above	0	10	20	30–50	50	70
	10,000–15,000	n/a	0–10 ¹⁾	0–20 ¹⁾	0–30 ¹⁾		
General cargo ship	15,000 and above	0	10	15	30		
	3,000–15,000	n/a	0–10 ¹⁾	0–15 ¹⁾	0–30 ¹⁾		
Refrigerated cargo carrier	5,000 and above	0	10	15	30		
	3,000–5,000	n/a	0–10 ¹⁾	0–15 ¹⁾	0–30 ¹⁾		
Combination carrier	20,000 and above	0	10	15	30		
	4,000–20,000	n/a	0–10 ¹⁾	0–15 ¹⁾	0–30 ¹⁾		

¹⁾ Obtaining X value by linear interpolation according to the size of the ship.

Table 2 X values of phase 3 of different container ship's size (IMO, 2020)

Size (DWT)	Phase 3
10,000–15,000	15–30 ¹⁾
15,000–40,000	30
40,000–80,000	35
80,000–120,000	40
120,000–200,000	45
over 200,000	50

¹⁾Obtaining X value by linear interpolation according to the size of the ship.

for each phase according to the year into the reference line value. The calculated values must satisfy the following equation. The X values are specified in Table 1. Since different values are applied to container ships depending on their size, they are listed in Table 2.

Attained EEDI \leq Required EEDI

$$= \left(1 - \frac{X}{100}\right) \times \text{Reference line value} \quad (1)$$

For Phase 4, however, the X value was set to 50, as regulations are reinforced, unlike in Phase 3. For the final target of 70% reduction, the reduction factor X value of Phase 5 was set to 70.

The Reference line value is obtained using Eq. (2) below, and the a , b , and c values can be obtained from Table 3.

Table 3 Reference line calculation parameters (IMO, 2011)

Ship type defined in Regulation 2	a	b	c
2.25 Bulk carrier	961.79	DWT	0.477
2.26 Gas carrier	1120.00	DWT	0.456
2.27 Tanker	1218.80	DWT	0.488
2.28 Container ship	174.22	DWT	0.201
2.29 General cargo ship	107.48	DWT	0.216
2.30 Refrigerated cargo carrier	227.01	DWT	0.244
2.31 Combination carrier	1219.00	DWT	0.488

Table 4 Carbon content and CF values of different fuel types (IMO, 2014)

Fuel type	Reference	Carbon content	C_F
1 Diesel/Gas oil	ISO 8217 Grades DMX ¹⁾ thorough DMB ¹⁾	0.8744	3.206
2 Light fuel oil (LFO)	ISO 8217 Grades RMA ¹⁾ thorough RMD ¹⁾	0.8594	3.151
3 Heavy fuel oil (HFO)	ISO 8217 Grades RME ¹⁾ thorough RMK ¹⁾	0.8493	3.114
4 Liquefied petroleum gas (LPG)	Propane	0.8182	3.000
	Butane	0.8264	3.030
5 Liquefied natural gas (LNG)		0.7500	2.750
6 Methanol		0.3750	1.375
7 Ethanol		0.5217	1.913

¹⁾The category of fuel, consisting of three letters: the first letter of this category is always the family letter (D for distillate or R for residual); the second letter, M, designates the application "Marine"; the third letter, X, A, B, C, ..., K, which indicates the particular properties in the product specification (ISO 8217)

$$\text{Reference line value} = a \times b^{-c} \quad (2)$$

The EEDI calculation formula and contents on the required coefficients are as follows:

$$\text{EEDI} = \frac{(P_{ME} \times C_{FME} \times SFC_{ME}) + (P_{AE} \times C_{FAE} \times SFC_{AE})}{\text{Capacity} \times V_{ref}} \quad (3)$$

P_{ME} : 75% of the rated installed power (Maximum continuous rating, MCR) for main engine (kW)

C_F : Conversion factor between fuel consumption and CO₂ emission (t-CO₂/t-fuel) (see Table 4)

SFC : Certified specific fuel consumption (g/kWh)

P_{AE} : Power of auxiliary engine (kW)

Capacity : Deadweight (DWT) (t)

V_{ref} : Ship speed, measured in nautical miles per hour (knot), in deep water under the condition corresponding to the capacity (nm/h)

Attained EEDI is obtained by substituting the corresponding coefficients of the target vessels into Eq. (3), and the reference line value is obtained using Eq. (2). After obtaining the required EEDI using Eq. (1), its satisfaction is examined through a comparison.

2.1.1 Main assumptions for calculation

Prior to the calculation of the index, certain coefficients were assumed for calculation because data from actual ships were not sufficient. The assumed values and grounds for them are as follows:

(1) P_{ME}

By referring to the main engine power of the target vessel selected in the capacity term below and the engine manufacturer data (MAN Energy Solutions, 2019), the dual fuel (fuel oil + methane) main engine with the most similar value was selected, and 75% of its maximum continuous rating (MCR) was selected.

(2) SFC

In the case of the main engine, since the specific fuel consumption

(SFC), specific gas consumption (SGC), and specific pilot oil consumption (SPOC) values at MCR 75% are specified, they were used as references.

In the case of the auxiliary engine, the SFC value was obtained by referring to the engine manufacturer data (MAN Energy Solutions, 2019). The SGC and SPOC of the auxiliary engine were calculated using the same ratio as the SFC ratio between the main and auxiliary engines.

(3) P_{AE}

P_{AE} can be obtained by multiplying P_{ME} by 0.025 and adding 250.

(4) Capacity

Among the actual ship data, DWT was designated as a range. DWT was determined for actual ships that can obtain the main engine power values within the range.

(5) V_{ref}

The operating speed for container ships and VLCC was set to V_{ref} .

2.2 Target Vessels

Here, the ship type, hull form, and size for target vessels were required to calculate the index. A 50K DWT KCS container ship and a 300K DWT KVLCC2 crude oil tanker, which are open hull forms, were selected as target vessels. Their detailed information is as follows:

(1) KCS container ship

- DWT: 55,387 t
- Actual main engine type: 8K98MC-C
- Actual main engine power: 34,071 kW
- Selected main engine type: MAN B&W, 5G95MEGI
- Selected main engine power: 34,350 kW (MCR)

(2) KVLCC2 crude oil tanker

- DWT: 309,097 t
- Actual main engine type: 7S70MC-C
- Actual main engine power: 24,446 kW
- Selected main engine type: MAN B&W, 7S70MEGI
- Selected main engine power: 24,010 kW (MCR)

Therefore, the vessels used for calculation were judged to be suitable for calculation because their size and engine power were identical or similar to those of actual ships.

2.3 Calculation Results

2.3.1 KCS container ship

First, the reference line value of the container ship is calculated using Eq. (2) and Table 2. The required EEDI at each phase can be calculated as follows. The unit is $\text{gCO}_2/\text{t} \cdot \text{nmile}$.

$$\text{Reference line value} = 174.22 \times 55387^{-0.201} = 19.394 \quad (4)$$

$$\text{Required EEDI}_{Ph2} = \left(1 - \frac{20}{100}\right) \times 19.394 = 15.515 \quad (5)$$

$$\text{Required EEDI}_{Ph3} = \left(1 - \frac{35}{100}\right) \times 19.394 = 12.606 \quad (6)$$

$$\text{Required EEDI}_{Ph4} = \left(1 - \frac{50}{100}\right) \times 19.394 = 9.697 \quad (7)$$

$$\text{Required EEDI}_{Ph5} = \left(1 - \frac{70}{100}\right) \times 19.394 = 5.818 \quad (8)$$

The attained EEDI was calculated for diesel and LNG modes in Eq. (9) and (10) of the main engine and auxiliary engines, respectively, and the results were compared with the required EEDI from Eq. (5) to (8) to check if the requirements were fulfilled.

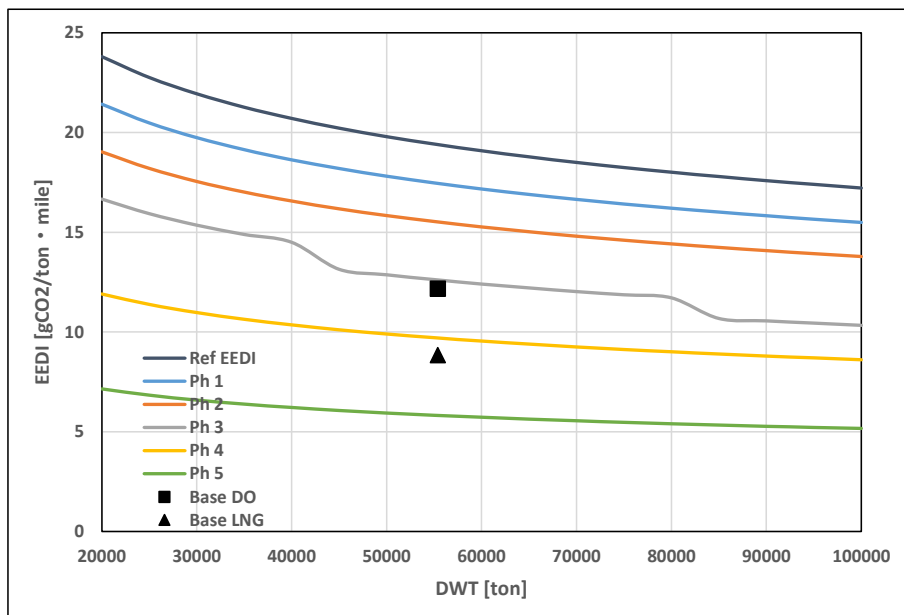


Fig. 1 Reference EEDI and Required EEDI of KCS container ship

$$Attained EEDI_{DO} = \frac{(25762.5 \times 3.206 \times 162.5) + (1108.75 \times 3.206 \times 204.9)}{55387 \times 21} = 12.166 \quad (9)$$

$$Attained EEDI_{LNG} = \frac{(25762.5 \times (3.206 \times 3.0 + 2.75 \times 134.125)) + (1108.75 \times (3.206 \times 3.811 + 2.75 \times 169.364))}{55387 \times 21} = 8.838 \quad (10)$$

Both the EEDI calculated using the above calculation results and the IMO regulations are shown in Fig. 1. For the container ship, Phase 1, 2, and 3 can be satisfied when diesel is used as fuel. To satisfy Phase 4 and above, additional measures must be applied. When LNG is used as fuel, however, regulations of up to Phase 4 can be complied with.

2.3.2 KVLCC2 crude oil tanker

For the KVLCC2 crude oil tanker, the following values from Eq. (11) to (17) can be obtained through the above index calculation process. The unit is $\text{gCO}_2/\text{t} \cdot \text{nmile}$.

$$Reference\ line\ value = 1218.80 \times 309097^{-0.488} = 2.551 \quad (11)$$

$$Required\ EEDI_{Ph2} = (1 - \frac{20}{100}) \times 2.551 = 2.041 \quad (12)$$

$$Required\ EEDI_{Ph3} = (1 - \frac{30}{100}) \times 2.551 = 1.786 \quad (13)$$

$$Required\ EEDI_{Ph4} = (1 - \frac{50}{100}) \times 2.551 = 1.276 \quad (14)$$

$$Required\ EEDI_{Ph5} = (1 - \frac{70}{100}) \times 2.551 = 0.7654 \quad (15)$$

$$Attained\ EEDI_{DO} = \frac{(18007.5 \times 3.206 \times 166.25) + (850.25 \times 3.206 \times 196.492)}{309097 \times 15} = 2.186 \quad (16)$$

$$Attained\ EEDI_{LNG} = \frac{(18007.5 \times (3.206 \times 3.1 + 2.75 \times 137.3)) + (850.25 \times (3.206 \times 3.656 + 2.75 \times 162.482))}{309097 \times 15} = 1.589 \quad (17)$$

After calculating the attained EEDI for the diesel and LNG modes in Eq. (16) and (17), respectively, the results were compared with the required EEDI from Eq. (12) to (15) to check if the requirements were fulfilled.

As observed in Fig. 2, only the requirements of Phase 1 can be fulfilled when the crude oil tanker is operated using diesel as fuel. Since the requirements of Phase 2 and above cannot be fulfilled, additional measures are required. Requirements of Phases 1, 2, and 3 can be fulfilled when LNG is used as fuel. Table 5 summarizes the calculation results for the two target vessels.

Table 5 EEDI calculation result

Calculated EEDI	KCS container ship	KVLCC2 crude oil carrier
Reference line value	19.39	2.55
Required EEDI Phase 2	15.52	2.04
Required EEDI Phase 3	12.61	1.79
Required EEDI Phase 4	9.69	1.28
Required EEDI Phase 5	5.82	0.77
Attained EEDI DO	12.17	2.19
Attained EEDI LNG	8.84	1.59

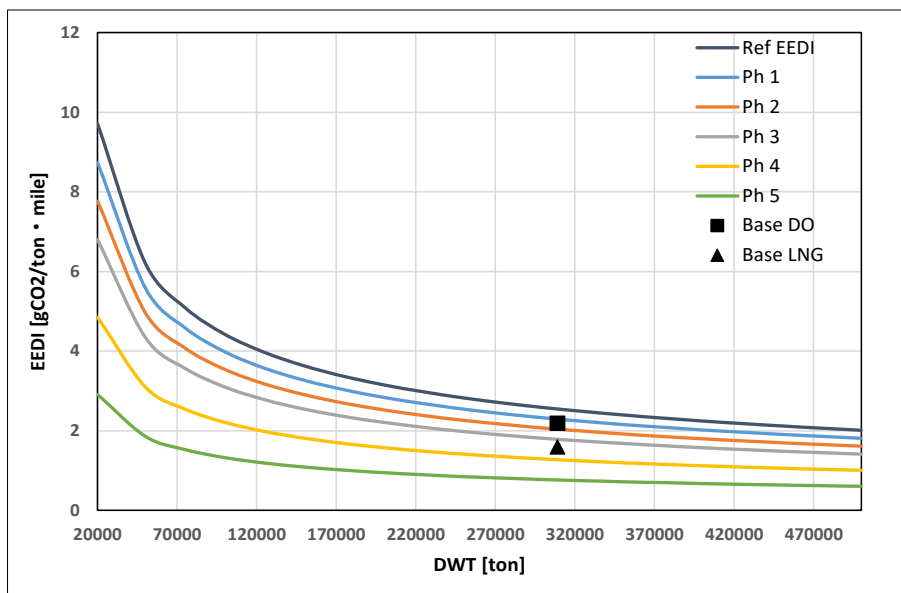


Fig. 2 Reference EEDI and Required EEDI of KVLCC2 crude oil tanker

2.4 Technical Measures for Improving EEDI

If the attained EEDI obtained for the target vessel is higher than the required EEDI, appropriate measures need to be taken to decrease it. Four main measures are available. The easiest method is to reduce the ship speed. In addition, methods for improving fuel efficiency through an improvement in propulsion efficiency by additionally mounting appendages on the hull or by reducing resistance through the modification of the bow shape and OCCS were considered.

2.4.1 Speed reduction

As mentioned above, the container ship can meet up to Phase 3 when operated using diesel as fuel. When the speed is lowered by decreasing 75% of MCR to 50%, the following values in Eq. (18) and (19) can also be obtained. The unit is $\text{gCO}_2/\text{t} \cdot \text{nmile}$. SS stands for slow steaming, implying deceleration.

Therefore, the container ship can meet up to Phase 4 (9.697) while operated using diesel by reducing its speed.

For the crude oil tanker, the following values in Eq. (20) and (21) can also be obtained when its speed is lowered to the MCR 50% condition as with the container ship.

As per the above results, the crude oil tanker can meet up to Phase 3 (1.786) when the speed is decreased and diesel fuel is used. If the fuel

is switched to LNG, Phase 4 requirements (1.276) can be fulfilled.

2.4.2 ESD installation

According to an ESD-related research report (KIOST, 2016), when LV-Fin (low viscous resistance fin), an energy-saving fin attached the stern, was applied to the KVLCC2 hull form, the effect of reducing delivered horsepower by approximately 1% was verified. When super stream duct (SSD) type ESD was installed, the effect of reducing delivered horsepower by more than 5% was predicted by CFD simulation, and the effect of reducing delivered horsepower by approximately 3% at the reference ship speed was confirmed through a model test. When duct-fin-combined ESD was installed, the effect of reducing delivered horsepower by approximately 7% was estimated, and the 4.1% reduction effect at the reference ship speed was verified through a model test. In addition, when a hybrid counter-rotating propeller (CRP) propulsion system was installed, the effect of reducing delivered horsepower by approximately 10% at the same ship speed was verified. When the propulsion efficiency improved by 5%, and 10% was applied at MCR 75% by referring to the above report, the attained EEDI of the target vessels was calculated by assuming that the effect of remodeling the bow shape is the same as the ESD installation effect.

$$\text{Attained EEDI}_{DO-SS} = \frac{(17175 \times 3.206 \times 159.125) + (1108.75 \times 3.206 \times 204.9)}{55387 \times 18} = 9.519 \quad (18)$$

$$\text{Attained EEDI}_{LNG-SS} = \frac{(17175 \times (3.206 \times 3.975 + 2.75 \times 132.525)) + (1108.75 \times (3.206 \times 3.811 + 2.75 \times 169.364))}{55387 \times 18} = 7.029 \quad (19)$$

$$\text{Attained EEDI}_{DO-SS} = \frac{(12005 \times 3.206 \times 163.875) + (850.25 \times 3.206 \times 196.492)}{309097 \times 13} = 1.703 \quad (20)$$

$$\text{Attained EEDI}_{LNG-SS} = \frac{(12005 \times (3.206 \times 4.025 + 2.75 \times 136.525)) + (850.25 \times (3.206 \times 3.656 + 2.75 \times 162.482))}{309097 \times 13} = 1.257 \quad (21)$$

$$\text{Attained EEDI}_{DO-ESD5} = \frac{(24474.38 \times 3.206 \times 162.5) + (1108.75 \times 3.206 \times 204.9)}{55387 \times 21} = 11.589 \quad (22)$$

$$\text{Attained EEDI}_{LNG-ESD5} = \frac{(24474.38 \times (3.206 \times 3.0 + 2.75 \times 134.125)) + (1108.75 \times (3.206 \times 3.811 + 2.75 \times 169.364))}{55387 \times 21} = 8.419 \quad (23)$$

$$\text{Attained EEDI}_{DO-ESD10} = \frac{(23186.25 \times 3.206 \times 162.5) + (1108.75 \times 3.206 \times 204.9)}{55387 \times 21} = 11.012 \quad (24)$$

$$\text{Attained EEDI}_{LNG-ESD10} = \frac{(23186.25 \times (3.206 \times 3.0 + 2.75 \times 134.125)) + (1108.75 \times (3.206 \times 3.811 + 2.75 \times 169.364))}{55387 \times 21} = 8.000 \quad (25)$$

$$\text{Attained EEDI}_{DO-ESD5} = \frac{(17107.13 \times 3.206 \times 166.25) + (850.25 \times 3.206 \times 196.492)}{309097 \times 15} = 2.082 \quad (26)$$

$$\text{Attained EEDI}_{LNG-ESD5} = \frac{(17107.13 \times (3.206 \times 3.1 + 2.75 \times 137.3)) + (850.25 \times (3.206 \times 3.656 + 2.75 \times 162.482))}{309097 \times 15} = 1.514 \quad (27)$$

$$\text{Attained EEDI}_{DO-ESD10} = \frac{(16206.75 \times 3.206 \times 166.25) + (850.25 \times 3.206 \times 196.492)}{309097 \times 15} = 1.979 \quad (28)$$

$$\text{Attained EEDI}_{LNG-ESD10} = \frac{(16206.75 \times (3.206 \times 3.1 + 2.75 \times 137.3)) + (850.25 \times (3.206 \times 3.656 + 2.75 \times 162.482))}{309097 \times 15} = 1.439 \quad (29)$$

$$Attained EEDI_{DO-SSED} = \frac{(16316.3 \times 3.206 \times 159.125) + (1108.75 \times 3.206 \times 204.9)}{55387 \times 18} = 9.080 \quad (30)$$

$$Attained EEDI_{LNG-SSED} = \frac{(17175 \times (3.206 \times 3.975 + 2.75 \times 132.525)) + (1108.75 \times (3.206 \times 3.811 + 2.75 \times 169.364))}{55387 \times 18} = 6.705 \quad (31)$$

$$Attained EEDI_{DO-SSES} = \frac{(11404.75 \times 3.206 \times 163.875) + (850.25 \times 3.206 \times 196.492)}{309097 \times 13} = 1.624 \quad (32)$$

$$Attained EEDI_{LNG-SSES} = \frac{(11404.75 \times (3.206 \times 4.025 + 2.75 \times 136.525)) + (850.25 \times (3.206 \times 3.656 + 2.75 \times 162.482))}{309097 \times 13} = 1.199 \quad (33)$$

For the container ship, the calculation were conducted as follows; 5% improvement with ESD using diesel and LNG in Eq. (22) and (23) and 10% in Eq. (24) and (25). The EEDI value cannot meet Phase 4 (9.697) with diesel fuel even when the propulsion efficiency is improved by ESD installation, indicating that the fuel must be changed.

The attained EEDI of the crude oil tanker was calculated as follows; 5% in Eq. (26) and (27) and 10% in Eq. (28) and (29) as same order as container's.

Phase 2 (2.041) requirements cannot be fulfilled with diesel fuel even when the propulsion efficiency is improved by 5% through ESD installation, indicating that a 10% efficiency improvement is required.

2.4.3 Application of both speed reduction and ESD installation

In Section 2.4.1, the index was calculated when the speed of each target vessel was reduced to MCR 50%. In Section 2.4.2, it was calculated by reflecting the ESD installation effect, and whether the results satisfied the regulations was examined. In Section 2.4.3, the index was calculated by reflecting both MCR 50% speed reduction and the 5% propulsion efficiency improvement effect through ESD installation, and the results are as follows; Eq. (30) and (31) are in diesel and LNG usage with slow steaming and ESD at the same time in container and Eq. (32) and (33) in VLCC.

For the container ship, Phase 4 (9.697) requirement is satisfied but Phase 5 (5.818) requirement is not fulfilled owing to the speed reduction effect discussed in Section 2.4.1. Therefore, additional measures are required.

As with the results of Section 2.4.1, the crude oil tanker meets Phase 3 (1.785) with diesel and Phase 4 (1.275) with LNG. It also requires additional measures to meet Phase 5 (0.7654).

2.4.4 OCCS

It was confirmed that up to Phase 4 requirement can be fulfilled through MCR 50% speed reduction and ESC installation. However, additional measures are required to prepare for the Phase 5 regulation. Here, considering the current situation where it is difficult to supply carbon-free fuel, the application of OCCS with high technological maturity was considered. To this end, a CO₂ capture process based on an monoethanolamine (MEA) aqueous solution was designed using Aspen Plus v10, a commercial process simulation software program. The process simulation was performed using a rate-based model. The electrolyte non-random two-liquid redlich-kwong (eNRTL-RK) equation of state was used to calculate the activity coefficient, Gibbs energy, enthalpy, and entropy of the MEA solution, and the perturbed-chain statistical associating fluid theory (PC-SAFT) model was used to calculate the fugacity coefficient of the gas phase.

The PC-SAFT model is a SAFT model that Gross and Sadowski developed by applying the Barker-Henderson perturbation theory to a hard-chain reference fluid. This model is represented by the residual Helmholtz free energy term (A^{res}) generated by interactions among molecules in different forms in a system and is equal to the value obtained by subtracting the Helmholtz free energy of the ideal gas at the same temperature and density (T and ρ). It consists of a hard-sphere-related term, a chain term, a dispersion-related term, and an

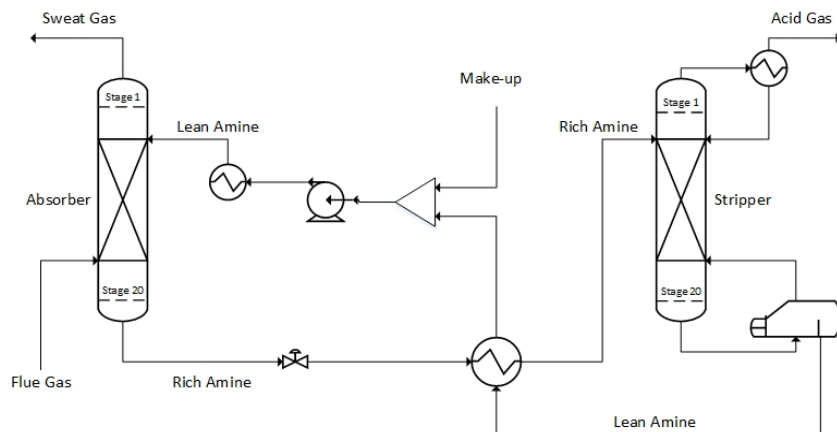


Fig. 3 Process flow diagram of on-board CO₂ capture process adopting the MEA (monoethanolamine) solution

association-related term (Gross et al., 2001; Diamantonis et al., 2013).

$$\begin{aligned} \frac{A^{res}(T, \rho)}{NRT} &= \frac{a^{res}(T, \rho)}{RT} = \frac{a(T, \rho)}{RT} - \frac{a^{ideal}(T, \rho)}{RT} \\ &= \frac{a^{ref}(T, \rho)}{RT} + \frac{a^{disp}(T, \rho)}{RT} \\ &= \frac{a^{hs}(T, \rho)}{RT} + \frac{a^{chain}(T, \rho)}{RT} + \frac{a^{disp}(T, \rho)}{RT} + \frac{a^{assoc}(T, \rho)}{RT} \end{aligned} \quad (34)$$

Fig. 3 shows the process flow diagram of OCCS below.

The process consists of an absorber that selectively removes CO₂ from the ship exhaust gas, a stripper that regenerates an aqueous amine solution, and a heat exchanger. The aqueous amine solution (lean amine) absorbs CO₂ contained in the exhaust gas while passing through the absorber. In this instance, the aqueous amine solution flows into the top of the tower, and the exhaust gas is introduced into the bottom of the tower to make counter-current contact. The aqueous amine solution that absorbed CO₂ (rich amine) is discharged from the top of the tower and introduced into the stripper via the heat exchanger. The aqueous amine solution is heated by the reboiler of the stripper to separate CO₂, which is discharged through the top of the stripper. The regenerated aqueous amine solution (lean amine) exchanges heat with rich amine at the heat exchanger and returns to the top of the absorber. Since a high-temperature condition of more than 120 °C is required to regenerate the aqueous amine solution in the stripper, OCCS is regarded as a system with high energy consumption. Therefore, optimal design of the absorber and stripper and the use of a heat exchanger is required to maximize its thermal efficiency. For carbon capture, a commonly used 30wt% MEA solution was used, and the carbon dioxide removal rate was set to 90%. The installation of OCCS may change the hull form or air resistance; however, such changes were not reflected here.

The CO₂ reduction rate and CO₂ reduction amount required to meet the Phase 5 regulation are shown in Table 6. For the absorber and stripper of OCCS that can be mounted on the container ship and crude oil tanker, the maximum and minimum sizes were calculated. As observed in Table 6, the maximum reduction amount occurred when the container ship used diesel as fuel, and the minimum reduction amount was observed when using LNG as fuel. MCR 50% speed reduction and 5% propulsion efficiency improvement effect through ESD installation for the container ship were considered simultaneously. Therefore, these two cases were set as the maximum and minimum sizes, and the column size was calculated. The following results show that the OCCS column size required for the crude oil tanker is within the maximum-minimum size range.

The diameters and heights of the absorber and stripper required for the above-mentioned CO₂ removal were calculated to estimate the approximate footprint of OCCS. As shown in Table 7, an absorber diameter of 3.51 m, an absorber height of 11.28 m, a stripper diameter of 1.52 m, and a stripper height of 9.60 m were calculated as the maximum size. An absorber diameter of 1.22 m, an absorber height of 11.28 m, a stripper diameter of 0.61 m, and a stripper height of 8.84 m

Table 6 CO₂ emissions and reduction target

Case	CO ₂ emissions (kg/h)	CO ₂ reduction rate (%)	CO ₂ reduction amount (kg/h)
Container base DO	14150.60	52.2	7386.61
LNG + SS + ESD	6684.66	13.3	889.06
VLCC Base DO	10135.29	65.0	6587.94
LNG + SS + ESD	4817.89	36.2	1744.08

Table 7 Result of CCS column size

Size	Absorber diameter (m)	Absorber height (m)	Stripper diameter (m)	Stripper height (m)
Max. size	3.51	11.28	1.52	9.60
Min. size	1.22		0.61	8.84

were calculated as the minimum size. Due to the nature of the ship structure, the calculation was performed in a direction to decrease the height and increase the diameter. The height of the stripper was confirmed to be low due to the small difference in lean-rich loading. However, the larger difference will lead to a lower flow rate, but the height of the absorber should increase. The removal rate was set to 90%, such that an appropriate height could be determined, and FLEXIPAC HC Structured Packing 250Y (KOCH-GLITSCH) was used as the packing material. In this instance, the energy required by the stripper for regeneration was calculated to be 3.07 GJ/tCO₂, indicating that the optimal design to increase thermal efficiency was attained. When the case of using diesel as fuel without considering any technical measures is compared with the case of applying technical measures, such as speed reduction and ESD installation, while using LNG as fuel based on the above results, the diameter decreases by approximately 60% despite no significant difference in height. In other words, various technical measures are required to satisfy EEDI, enabling the compact design of OCCS.

3. Results and Discussion

Main engines were selected considering a container ship and a crude oil tanker under KCS and KVLCC2 hull form conditions. The EEDI

Table 8 Comparison of EEDI calculation result

Case	KCS		KVLCC2	
	DO	LNG	DO	LNG
Base	12.166	8.838	2.186	1.589
SS (Slow steaming)	9.519	7.029	1.703	1.257
ESD (DHP 5%)	11.589	8.419	2.082	1.514
ESD (DHP 10%)	11.012	8.000	1.979	1.439
SS + ESD (DHP 5%)	9.08	6.705	1.624	1.199

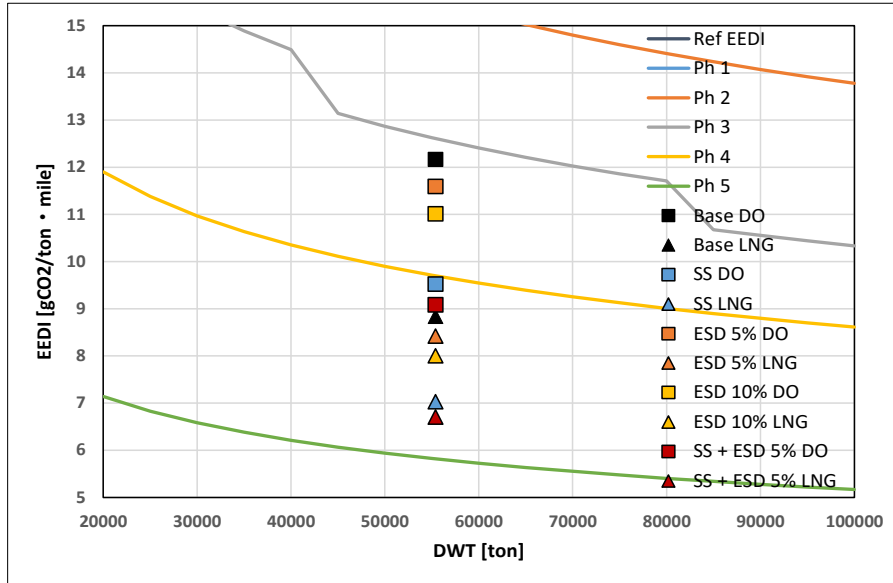


Fig. 4 Result of required EEDI and attained EEDI with actions taken on the KCS container ship

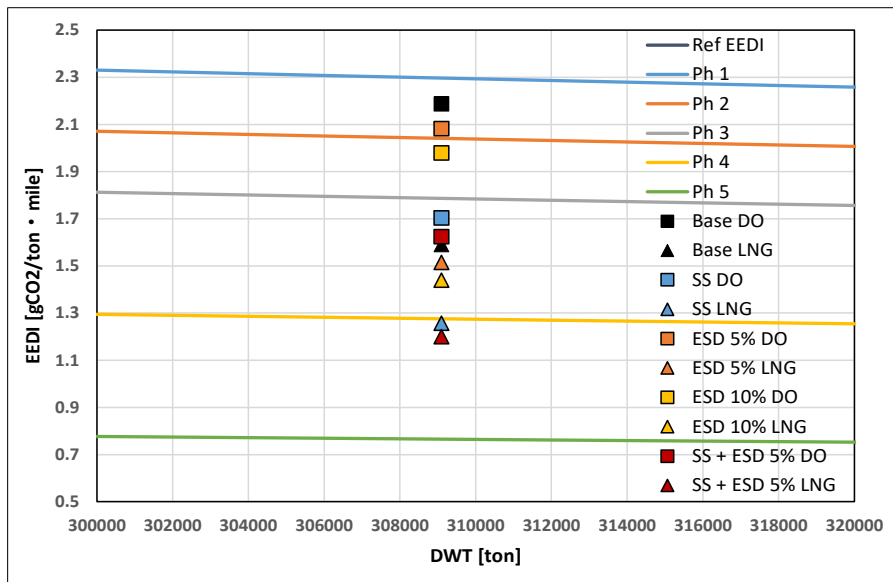


Fig. 5 Result of required EEDI and attained EEDI with actions taken on the KVLCC2 crude oil tanker

calculation results according to the conditions of speed reduction, ESD installation, and both speed reduction and ESD installation and the fuel type are summarized in Table 8. EEDI was calculated to be 26.86% lower on average for LNG compared with diesel. The fuel change from diesel to LNG exhibited the largest reduction in EEDI, followed by decreasing the ship speed among additional measures. The reduction can be increased through ESD installation. To meet the Phase 5 regulation, OCCS can be a potential alternative for the target vessels. Fig. 4 shows the EEDI calculation results obtained from KCS. The EEDI calculation results obtained from KVLCC2 are shown in Fig. 5.

4. Conclusion

Here, ships that applied the target hull forms and their main engines

were selected, and the energy efficiency design index (EEDI) was calculated under the conditions of speed reduction, ESD installation, and both speed reduction and ESD installation.

(1) When diesel fuel was used under basic conditions, the KCS hull form fulfilled the requirements of up to Phase 3 while the VLCC2 hull form fulfilled the requirements of Phase 1 in terms of the required EEDI.

(2) When LNG fuel was used under basic conditions, the KCS hull form satisfied the requirements up to Phase 4, and the VLCC2 hull form up to Phase 3.

(3) For each target hull form, the fuel change from diesel to LNG exhibited the largest EEDI reduction effect. Among additional measures, decreasing the ship speed resulted in the largest EEDI reduction effect, except for onboard carbon capture and storage

(OCCS).

(4) The EEDI can be secured economically through speed reduction, and the IMO regulations can be satisfied at low cost if speed reduction, ESD, and fuel change can be appropriately applied to the ships according to the regulation phase. It is judged, however, that the installation of OCCS must be considered for the Phase 5 regulation, which is the final goal.

(5) Further research is required in the future to optimize the size and energy consumption of OCCS.

For effective response to carbon emission regulations, complex analysis considering and applying various measures and subsequently examining their effects is required. Moreover, since the analysis method can be more complicated when the characteristics of ships are added, further research needs to be conducted to derive further enhanced improvement measures.

Conflict of Interest

No potential conflict of interest relevant to this article was reported.

Funding

This work received no specific grant from any funding agency in the public, commercial, or not-for-profit sectors.

References

- Choi, J. S., & Rho, B. S. (2011). A Study on the Energy Efficiency Operational Indicator for CO₂ Reduction from Ships. *Journal of Advanced Marine Engineering and Technology*, 35(8), 1035–1040.
- Diamantonis, N. I., Boulougouris, G. C., Mansoor, E., Tsangaris, D. M., & Economou, I. G. (2013). Evaluation of cubic, SAFT, and PC-SAFT equations of state for the vapor–liquid equilibrium modeling of CO₂ mixtures with other gases. *Industrial & Engineering Chemistry Research* 2013, 52(10), 3933–3942. <https://doi.org/10.1021/ie303248q>
- Gross, J., & Sadowski, G. (2001). Perturbed-Chain SAFT: An equation of state based on perturbation theory for chain molecules. *Industrial & Engineering Chemistry Research* 2001, 40(4), 1244–1260. <https://doi.org/10.1021/ie0003887>
- International Maritime Organization (IMO). (2022). Reduction of GHG emissions from ships; Proposal for including carbon capture technologies in the IMO regulatory framework to reduce GHG emissions from ships. MEPC 79/7.4.
- International Maritime Organization. (2011). Amendments to the ANNEX of the protocol of 1997 to amend the international convention for the prevention of pollution from ships, 1973, as modified by the protocol of 1978 relating thereto (Resolution MEPC.203(62)).
- International Maritime Organization. (2014). 2014 Guidelines on the method of calculation of the attained Energy Efficiency Design Index(EEDI) for new ships (Resolution MEPC.245(66)).
- International Maritime Organization. (2018). 2018 Guidelines on the method of calculation of the attained Energy Efficiency Design Index(EEDI) for new ships (Resolution MEPC.308(73)).
- International Maritime Organization. (2020). Amendments to the ANNEX of the protocol of 1997 to amend the international convention for the prevention of pollution from ships, 1973, as modified by the protocol of 1978 relating thereto (Resolution MEPC.324(75)).
- Jung, J. Y., & Seo, Y. T. (2022). Onboard CO₂ capture process design using rigorous rate-based model. *Journal of Ocean Engineering and Technology*, 36(3), 168–180. <https://doi.org/10.26748/KSOE.2022.006>
- Jung, K.H. (2014). *Study of various effects and CO₂ absorption on EEDI (Energy efficiency design index) in merchant ships* [Master's Thesis, Pohang University of Science and Technology]. https://postech-primo.hosted.exlibrisgroup.com/permalink/f/qubeit/82POSTECH_INST2190081700003286
- Kim, J. H., Choi, J. E., Choi, B. J., Chung, S. H., & Seo, H. W. (2015). Development of energy-saving devices for a full slow-speed ship through improving propulsion performance. *International Journal of Naval Architecture and Ocean Engineering*, 7(2), 390–398. <https://doi.org/10.1515/ijnaoe-2015-0027>
- Korea Institute of Ocean Science & Technology (KIOST). (2016). *에너지 절감을 위한 선박 저항감소 및 추진성능 향상 핵심기술 개발* [Development of core technologies for reducing ship resistance and improving propulsion performance for energy saving]. <https://scienceon.kisti.re.kr/srch/selectPORSrchReport.do?cn=TRKO201800039492>
- MAN Energy Solutions. (2019). *Marine engine programme* 2018 (2nd ed.).
- Park, G., & Cho, K. (2017). A study on the change of EEOI before and after modifying bulbous at the large container ship adopting low speed operation. *Journal of Advanced Marine Engineering and Technology*, 41(1), 15–20.
- Shin, H. J., Lee, K. H., Han, M. R., Lee, C. Y., & Shin, S. C. (2013). Pre-swirl duct of fuel oil saving device design and analysis for ship. *Journal of the Society of Naval Architects of Korea*, 50(3), 145–152. <https://doi.org/10.3744/SNAK.2013.50.3.145>
- Song, H. J., Kim, M. C., Lee, W. J., Lee, K. W., & Kim, J. H. (2015). Development of the new energy saving device for the reduction of fuel of 176k bulk carrier. *Journal of the Society of Naval Architects of Korea*, 52(6), 419–427. <https://doi.org/10.3744/SNAK.2015.52.6.419>

Author ORCIDs

Author name	ORCID
Park, Junyup	0000-0002-6747-1806
Jeong, Jongyeon	0000-0002-7557-6587
Seo, Yutaek	0000-0001-8537-579X

Field Observation and Quasi-3D Numerical Modeling of Coastal Hydrodynamic Response to Submerged Structures

Yejin Hwang¹, Kideok Do², Inho Kim³ and Sungeol Chang⁴

¹Master Course, Department of Convergence Study on the Ocean Science and Technology, Korea Maritime and Ocean University, Busan, Korea

²Associate Professor, Department of Ocean Engineering, Korea Maritime and Ocean University, Busan, Korea

³Professor, Department of Earth and Environmental Engineering, Kangwon National University, Samcheok, Korea

⁴Director, Haeyeon Engineering and Consultants Corporation, Gangneung, Korea

KEYWORDS: Simulating waves till shore (SWASH), Quasi-3D model, Submerged breakwater, Bongpo Beach, Storm wave

ABSTRACT: Even though submerged breakwater reduces incident wave energy, it redistributes the coastal area's wave-induced current, sediment transport, and morphological change. This study examines the coastal hydrodynamics and the morphological response of a wave-dominated beach with submerged breakwaters installed through field observation and quasi-3D numerical modeling. The pre-and post-storm bathymetry, water level, and offshore wave under storm forcing were collected in Bongpo Beach on the East coast of Korea and used to analyze the coastal hydrodynamic response. Four vertically equidistant layers were used in the numerical simulation, and the wave-induced current was examined using quasi-3D numerical modeling. The shore normal incident wave (east-northeast) generated strong cross-shore and longshore currents toward the hinterland of the submerged breakwater. However, the oblique incident wave (east-southeast) induced the southeastward longshore current and the sedimentation in the northeast area of the beach. The results suggested that the incident wave direction is a significant factor in determining the current and sediment transport patterns in the presence of the submerged breakwaters. Moreover, the quasi-3D numerical modeling is more appropriate for estimating the wave transformation, current, and sediment transport pattern in the coastal area with the submerged breakwater.

1. Introduction

Submerged breakwaters (SBWs) are coastal structures commonly used to block high waves, i.e., the main external force of coastal erosion, and maintain coastal landscapes. In South Korea, several SBWs have been installed to respond to increased frequency of high waves caused by storms and erosion caused by artificial development. However, SBWs, change the wave energy environment on the coast and cause an increase in water level and changes in wave-induced currents in the hinterland of SBWs, thereby significantly affecting sediment transport in nearby waters and coastline changes (Ranasinghe et al., 2010; Villani et al., 2012). In particular, wave breaking occurs around SBWs, making their prediction one of the challenges in the field of coastal engineering. Such wave breaking causes unexpected erosion in 60% of the coastal areas with SBWs (Ranasinghe and Turner, 2006) and occurs frequently on the east coast of Korea. Thus, to minimize the side effects of installing SBWs,

understanding the coastal physical environment after their installation is essential. In this regard, various studies have been conducted through field observation and hydraulic model experiments. In particular, several studies on the transmission rate of the waves generated in the open sea to the hinterland caused by SBWs have been conducted in two-dimensional (2D) hydraulic model water tanks (Lorenzoni et al., 2012; Marin and Savov, 2017; Walmsley et al., 2002), but the flow in the coastal direction and the diffraction of waves caused by SBWs cannot be considered. Haller et al. (2002) explained that the flow generated between SBWs dominates the flow pattern in the hinterland of SBWs and near the coastline through a three-dimensional (3D) hydraulic model experiment. Ranasinghe et al. (2010) and Ranasinghe et al. (2006) analyzed the experiment results of previous studies (Dean et al., 199; Groenewoud et al., 1996; Nobuoka et al., 1996) and presented the pattern of the circulation flow (2-cell circulation, 4-cell circulation) that appears as wave breaking dissipates behind SBWs. The latter proposed that the flow's pattern is

Received 26 December 2022, revised 26 January 2023, accepted 13 February 2023

Corresponding author Kideok Do: +82-51-410-5248, kddo@kmou.ac.kr

© 2023, The Korean Society of Ocean Engineers

This is an open access article distributed under the terms of the creative commons attribution non-commercial license (<http://creativecommons.org/licenses/by-nc/4.0>) which permits unrestricted non-commercial use, distribution, and reproduction in any medium, provided the original work is properly cited.

determined by the location and dimensions of the structure (width and crest height of SBWs) as well as incident waves from the open sea, which are major factors that cause the advance and retreat of the coastline. However, they had limitations in spatially observing complex phenomena that occur around SBWs comprehensively, with studies actively conducted worldwide on the development and advancement of numerical modeling techniques to evaluate the changes in waves, currents, and topography caused by the installation of SBWs in advance (Johnson et al., 2005; Liang et al., 2015; Magdalena et al., 2020; Quataert et al., 2020). However, previous studies reproduce the coastal flow, sediment transport, and topographic changes caused by SBWs through a 2D precision model to simulate the attenuation of the waves caused by SBWs and a planar model based on water depth integration and wave-governing equations. In this study, the simulating waves till shore (SWASH) model was used to simulate flow velocity by dividing layers in the vertical water-depth direction and accurately simulate the flow in the coastal area where the dissipation of wave-breaking is important or in front of and behind SBWs compared to planar models (Smit et al., 2013). Suzuki et al. (2011) and Liang et al. (2015) compared simulation results with water tank experiment results to examine the applicability of the SWASH model to coastal areas where artificial structures are installed. The wave transformation and overtopping caused by SBWs were well simulated; however, only the effects in the vertical direction were considered in both studies. Rathnayaka and Tajima (2020) compared flow field simulation results around SBWs with hydraulic experiment results to evaluate the reproducibility of the SWASH model for the single-layer mode and two-layer mode and concluded that complex wave changes and flows behind SBWs are better simulated in the two-layer mode. Da Silva et al. (2022) examined the influence of SBWs on coastal flow and wave runup using the SWASH model and explained that the average flow pattern that occurs on the coast could be used as a means of predicting the sediment transport pattern. In Korea, the flow characteristics of coastal wave-induced currents were analyzed using the SWASH model (Jang et al., 2014; Kang et al., 2015; Lee et al., 2015); however, the analysis was conducted by applying single-layer models to the beach with no SBW.

In this study, SWASH, a quasi-3D numerical model that can simulate vertical and horizontal flows simultaneously, was used to precisely simulate wave transformation and coastal flow in the event of a typhoon (Zijlema et al., 2011). The simulation results were indirectly compared using topographic change observation data before and after a typhoon. To this end, observation data acquired from Bongpo Beach were used, with erosion and deposition patterns in Bongpo Beach analyzed through wave series dominant on the beach during typhoon and the water depth difference by section before and after a typhoon. Considering it is difficult to identify mechanisms that cause sediment transport and topographic changes using observation data alone in Bongpo Beach, where several structures, including SBWs, are installed, the coast where SBWs were installed was divided

into four layers in the vertical direction, with flow simulation was performed for each layer. The analysis of the flow field and wave transformation results of the depth layer that dominantly causes topographic changes among the simulation results confirmed that the coastal flow was different depending on the incident wave conditions. Bongpo Beach was divided into sections for effective analysis, and wave conditions that dominantly cause topographic changes were proposed.

2. Target Sea Area and Observation Data

2.1 Study Area

In this study, data was collected through field observation, with numerical simulation performed to investigate phenomena using the data for Cheonjin-Bongpo Beach, where coastal maintenance projects were performed and SBWs were installed due to continuous coastal erosion after the construction of Cheonjin Port. Cheonjin-Bongpo Beach is inclined by approximately 45 degrees from the north and open to the northeast in the form of a beak, with waves more dominant than tides (Fig. 1). The total coastline length is 1.15 km, with the beach mostly comprising sand. After coastal maintenance projects, the average median particle diameter (D_{50}) was approximately 0.7 mm. The tidal range is approximately 18 cm and the influence of tidal currents is limited. The introduction of east-northeast (ENE) waves perpendicular to the coastline is dominant. The port located to the north of this beach is Cheonjin and the port to the south is Bongpo. The beaches in the middle are also divided into Cheonjin and Bongpo Beach, but they are collectively referred to as Bongpo Beach in this study. The target sea area had continuous erosion problems due to the construction of the ports and installation of revetment and was thus designated as an area subjected to erosion grade evaluation in surveys on coastal erosion since 2005. The evaluation is performed based on the monitoring grade evaluation criteria of the Ministry of Oceans and Fisheries, with four grades dependent on the evaluation results: A (excellent), B (moderate), C (concerned), and D (serious). Concerning Bongpo Beach, the extension of breakwaters in Cheonjin Port and the construction of coastal roads were analyzed as the causes of erosion. Bongpo Beach was continuously classified as grades C and D from 2010 to 2016, indicating that the sandy beach and hinterland are vulnerable to disasters. Accordingly, coastal maintenance projects, including installation of SBWs and beach nourishment, were performed every year from 2016 to 2019 as countermeasures against erosion. Consequently, three SBWs with a length of 150 m and a width of 40 m were installed on the front of the beach, located at 50 cm below sea level. The distance between them is approximately 80 m, with all of them located approximately 110 m from the coastline. The average beach width before the coastal maintenance projects was found to be approximately 35 m for Cheonjin and 28 m for Bongpo Beach. After the projects, the widths increased to approximately 44 and 35 m. Upon project completion, Cheonjin Beach was still classified as grade C, but Bongpo Beach was classified as grade A due

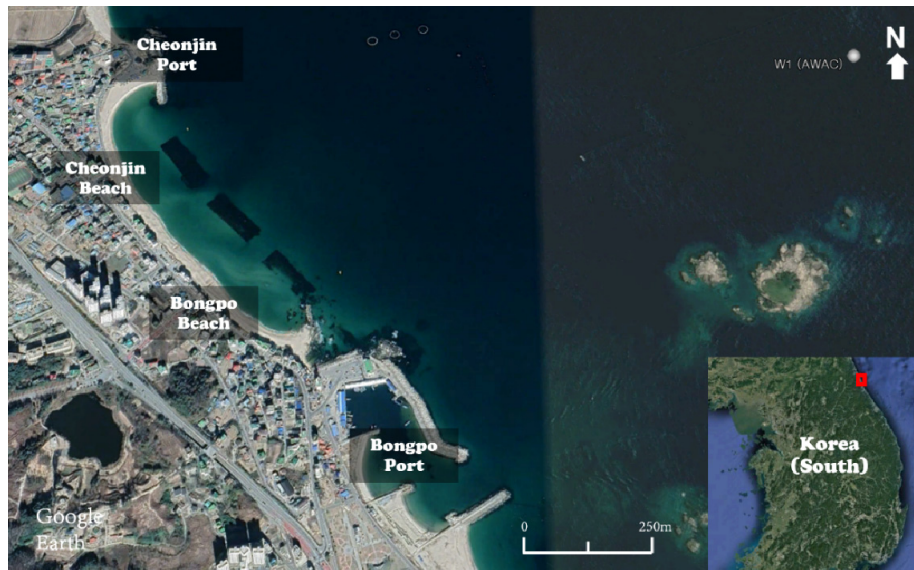


Fig. 1 Study area location (Bongpo Beach) with observation points, W1 (from Google Earth).

to the change in coastal sediment caused by the SBWs in the assessment performed in 2021. However, erosion still occurs due to summer typhoons and large height swell-like waves in winter.

2.2 Wave Data During the Typhoon Period

Wave observation was performed every hour from April 2020 to March 2021 by installing acoustic waves and currents (AWAC) at the mean sea level (MSL) (-) 25 m point (Fig. 1, W1). Fig. 2(a) shows the data from August 1 to October 1, 2020, when high waves occurred due to a typhoon in time series. When the significant wave height (H_s), peak period (T_p), peak wave direction (D_p), and wave rose during the entire observation period were analyzed, it was found that ENE waves were dominant (Fig. 2(b)). In the wave time-series data, Typhoon Maysak on September 3, 2020, which caused sand loss to the open sea and topographic changes in Bongpo Beach, is included. In this study, sediment transport and topographic change patterns in the SBW opening and hinterland by storm waves were analyzed using wave data and topographic observation data. Typhoon Maysak, with a minimum central pressure of 935 hPa and a maximum wind speed of 50–55 m/s, caused severe damage to the coastal areas of the East Sea, South Sea, and Jeju Island. At the wave observation point installed in Bongpo Beach, a maximum significant wave height of 5.43 m was observed, with a peak period of 10.01s. When the period during which Typhoon Maysak affected Bongpo Beach was analyzed in detail, both east-southeast (ESE) and ENE waves were found to be dominant (Fig. 2(c)). ENE waves perpendicular to the coastline of Bongpo Beach, were dominant, with a high proportion of 50%. However, a relatively low significant wave height of 3 m or less was observed. In contrast, ESE waves oblique to the coastline included several significant wave heights of 3 m or higher, even though their frequency was lower (a proportion of 40%) compared to ENE waves. This wave direction distribution affected waves by varying the wind direction according to the direction of Typhoon Maysak and its center location (Fig. 2(d)); it

is considered that high ESE waves caused sediment transport and topographic changes different from large height swell-like waves in winter.

2.3 Water Depth Data Before and After Storm Waves

Water depth observation was performed using an echo sounder (AquaRuler 200S, SonarTech) and a high-precision global navigation satellite system (GNSS) installed in a ship from MSL (-) 14 m to the MSL point. In addition, for the area from MSL to MSL (+) 5 m, including the coastline, data were acquired using real-time kinematic (RTK)-GNSS while moving along the coastline on foot with transportation equipment. In the case of Bongpo Beach, as almost no topographic change occurs outside MSL (-) 10 m, the depth of closure is judged to be approximately MSL (-) 10 m (Lim et al., 2021). Six observations were performed at 5 m or 10 m intervals to analyze the topographic changes caused by storm waves and high waves from July 2020 to March 2021. Five periods were analyzed based on the water depth observation time points, as shown in Table 1, classified into three erosion (E) periods when topographic changes are expected under the influence of high significant wave heights and two stabilization periods when beach stabilization is confirmed after high wave. In this study, the water depth data of the E1 period, which showed sand loss and topographic changes due to Typhoon Maysak after beach stabilization, were analyzed. When the water depth data before (August 25, 2020) and after (September 6, 2020) the typhoon were compared, it appears that the sand eroded near the coastline was transported and deposited in the hinterland of SBWs, which ranged from MSL (-) 4 m to MSL (-) 2 m. The sand volume, calculated where the water depth difference before and after the typhoon, was significant in analyzing the transport path of the lost sand in detail. Moreover, Bongpo Beach was divided into three sections to ensure that the difference between the erosion and deposition amounts could be minimized (Fig. 3). In this instance, the difference between the

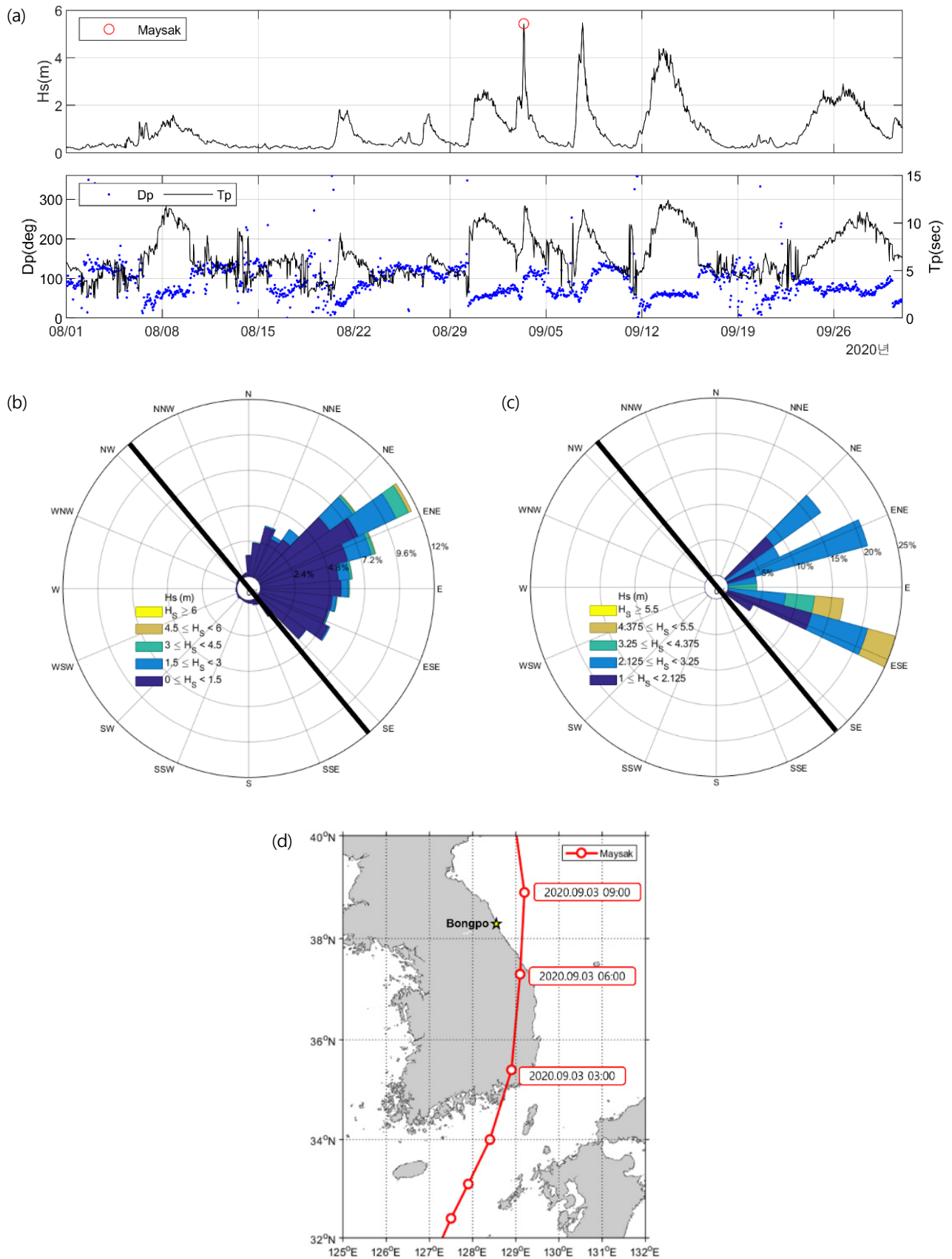
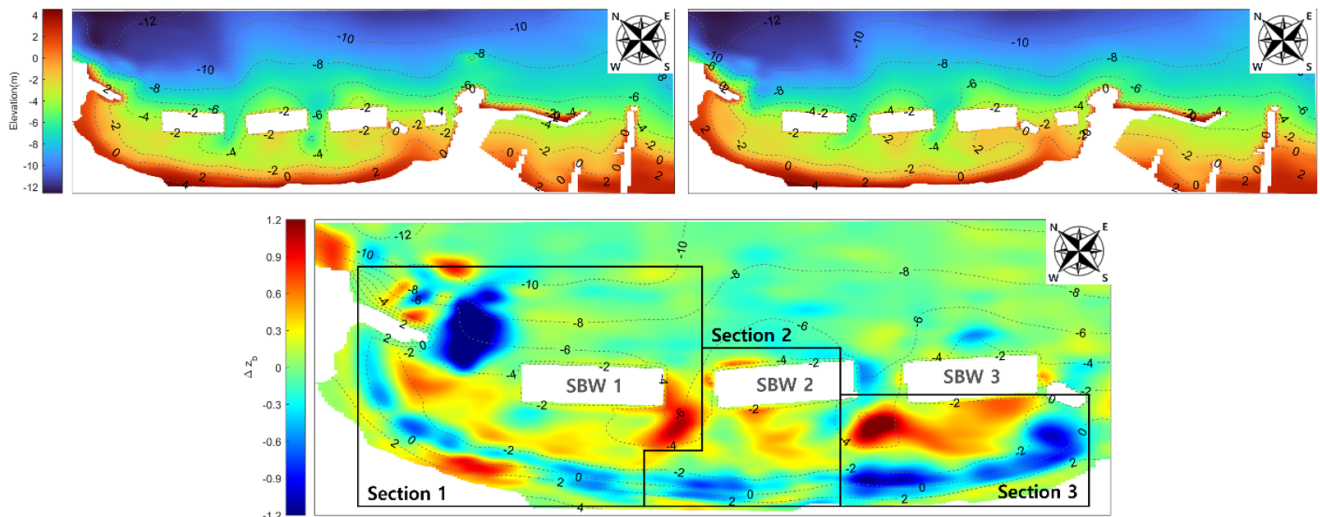


Fig. 2 Wave and typhoon data (a) Wave data in time-series collected during Aug.–Oct., 2020 (significant wave height, peak period, peak direction at W1), (b) Wave rose during Apr., 2020–Mar., 2021, (c) Wave rose during typhoon Maysak, and (d) Path of typhoon Maysak with a time of arrival in Korea (KMA, 2020).

Table 1 Summary of observation data from 29 August–30 October 2019

Period	Time interval between bathymetric survey (day)	Average during each period		
		H_s (m)	T_p (s)	D_p (degree)
S1	2020/07/08–2020/08/25 (49)	0.5	5.7	93.5
E1	2020/08/25–2020/09/06 (13)	1.1	7.0	94.6
E2	2020/09/06–2020/09/10 (5)	1.4	7.2	96.6
S2	2020/09/10–2020/11/24 (76)	0.9	6.3	62.7
E3	2020/11/24–2021/03/08 (105)	1.1	7.5	72.3

**Fig. 3** Bathymetry of Bongpo Beach Top: Bottom topography before and after the typhoon Maysak; Bottom: Elevation difference (Δz_b) of measured bed level between Aug. 25 and Sep. 6, 2020, indicating positive value (accretion) and negative value (erosion).**Table 2** Erosion and accretion volume and volume difference in each section

Volume (m^3)	Section 1	Section 2	Section 3
Erosion volume	14,563	4,025	10,831
Accretion volume	16,619	4,759	9,151
Difference	2,056	734	1,680

erosion and accretion volumes was approximately 2,000 m^3 in each section. Table 2 shows the volumes and volume differences in each section. In sections 2 and 3, the sand lost from the coastline is estimated to be deposited in the hinterland of SBWs 2 and 3. In the case of section 1, which shows complex water depth differences in many areas, there are limitations in predicting phenomena using observation data alone. Therefore, for the section, it is deemed necessary to analyze erosion and accretion patterns considering wave conditions that cause topographic changes and flow simulation results.

2.4 Flow Patterns in the Hinterland of SBWs

As aforementioned, the circulation flow pattern is determined by the distance between the coastline and SBWs and incident wave conditions on the coast where SBWs are installed. Fig. 4 briefly shows the patterns of coastal currents that may occur in the hinterland of

SBWs, which were discussed in previous studies (Ranasinghe et al., 2010; Ranasinghe and Turner, 2006). First, when the phenomenon that waves pass through SBWs and proceed to the hinterland is dominant, the water level of the hinterland rises, making the flow from the openings of the SBWs toward the open sea dominant, thereby generating two symmetrical circulation flows (2-cell current pattern) (Fig. 4(a)). In contrast, when the energy of waves is significantly dissipated while passing over SBWs, the flow in a direction parallel to the coastline becomes dominant, with four strong symmetrical circulation flows occurring in the hinterland of the SBWs, where wave energy is relatively low (4-cell current pattern) (Fig. 4(b)). In the 2-cell pattern, the erosion of the hinterland is induced because sand is transported from the hinterland to the openings of the SBWs. As for the 4-cell pattern, the accretion of the hinterland is dominant because the sand at the openings of the SBWs is transported to the hinterland. All flows shown in Fig. 4 are circulation patterns caused by normal incident waves. Oblique incident waves cause the development of longshore currents due to the direction of waves in the hinterland, while asymmetrical circulation flows significantly affected by the direction of longshore currents occur at erosion and accretion points (Ranasinghe et al., 2006).

Analyzing the topographic observation data, it was found that erosion near the coastline was dominant for Bongpo Beach due to Typhoon Maysak. It is estimated that ENE waves, which are

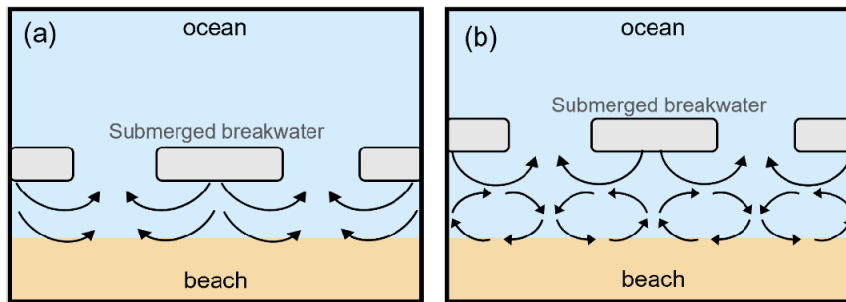


Fig. 4 Patterns of nearshore circulation (a) 2-cell and (b) 4-cell circulation patterns. Arrows denote wave-averaged (mean) flow patterns.

perpendicular to the coastline, formed the 2-cell circulation pattern in section 2 where SBW 2 was installed, thereby causing erosion from the hinterland and accretion in the opening (Fig. 3). Simultaneously, through the erosion point deflected to the northwest (NW) from the central part of the hinterland of SBW 2, it is considered that ESE waves formed asymmetrical circulation flows by developing strong NW longshore currents in the hinterland of SBW2. Notably, the Cheonjin Port breakwater generated southeast (SE) longshore currents in the hinterland of SBW 1 by causing reflected and diffracted waves in section 1, and the reflected waves by the jetty installed on the southeast side of SBW 3 generated NW longshore currents in the hinterland of SBW 3 in section 3, indicating that these two flows only strengthened the flow toward the openings of the SBWs.

3. Numerical Model Introduction and Input Data

3.1 SWASH Model

In this study, the SWASH model developed was based on the research by Smit et al. (2013), Stelling and Duinmeijer (2003), Stelling and Zijlema (2003), Zijlema and Stelling (2008), Zijlema et al. (2011), and Zijlema and Stelling (2005) and was used to identify the flow characteristics of Bongpo Beach under storm wave conditions. The SWASH model simulates hydrodynamic processes (e.g., nonlinear waves, rotational flows, and energy and sediment transport phenomena) caused by wave transformation on the coast; its governing equations are nonlinear shallow water equations that include a non-hydrostatic pressure term based on the Navier–Stokes equations. The SWASH model uses the approximation of linear dispersion and simulates the flow of layers in the vertical direction by performing wave transformation calculations with improved accuracy. This model also calculates the energy dissipation caused by wave breaking and effectively reproduces the characteristics of nonlinear waves under wave-breaking conditions, making it suitable for large-scale storm wave and high wave calculations.

3.2 Grid and Model Construction

The simulation domain included all areas from Cheonjin to Bongpo Port, considering ESE storm waves that interact with the latter Port as oblique incident waves toward the coastline. For efficient calculation, 244 (cross-shore) \times 289 (alongshore) variable grids were formed (Fig.

5). Different grid resolutions were applied depending on the section considering stabilization conditions. First, in the case of the cross-shore direction, the grid was constructed so that the grid size could range from 2–4 m near the open sea and 0.9–1.2 m near the surf zone and SBWs. In the case of the alongshore direction, the grid size ranged from 3.6–5 m for Bongpo Beach (where SBWs were installed) and 6–10 m for other areas, indicating a smaller grid size for the area of interest with SBWs.

The number of layers in the vertical direction significantly impacts computation times. In this study, four layers were divided considering the distance between the SBWs located in Bongpo Beach and the sea level is approximately 50 cm. The water depth data before the occurrence of Typhoon Maysak was used for bottom boundary conditions (Fig. 5), with the porosity coefficient set in the grid cells where SBWs were located regardless of the layers. For the physical coefficients and input conditions required in the numerical simulation, the default values presented in the SWASH model user manual were used as presented in Table 3 (SWASH team, 2020). Next, the diameter of the structure's size was applied. The significant wave height (H_s), peak period (T_p), and peak wave direction (D_p) data were used as open-sea wave boundary conditions, with the input reduction tool (Deltares, 2017) applied for the wave data during the typhoon period. A total of ten representative wave conditions (Table 4) were created, with the 2D Joint North Sea wave project (JONSWAP) spectrum simulated every 30 minutes. To minimize reflection in the open sea boundary, except for the incident wave boundary, a sponge layer with

Table 3 Computational information and physics of SWASH model

	Information	
Grid size	Cross-shore	0.94 m
	Alongshore	3.6–10 m
Vertical layer		4 layer
Simulation time		2 h
Spectrum		JONSWAP
Porosity structure	Size	3.0 m
	Alpha 0	200
	Beta 0	1.1
Bottom friction		0.019 m ² /s ³
Water density		1,025 kg/m ³
Gravitational acceleration		9.81 m/s ²

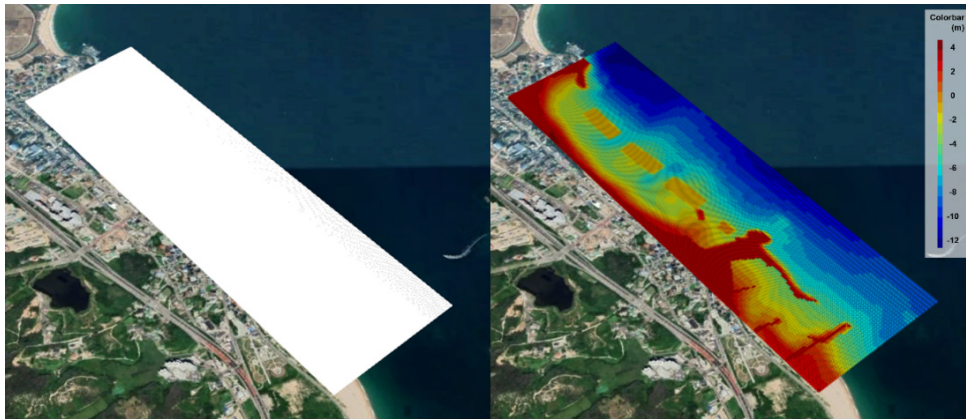


Fig. 5 Computational domain of curvilinear grid and depth for SWASH modeling.

Table 4 Wave condition for SWASH modeling

Case	Wave condition				Series
	H_s (m)	T_p (s)	D_p (degree)	Proportion	
1	2.22	6.8	53.1	0.21	ENE
2	2.25	6.5	70.2	0.17	ENE
3	1.59	10.2	110.5	0.17	ESE
4	2.7	11.5	99.4	0.08	ESE
5	2.33	11.3	106.9	0.08	ESE
6	4.17	8.4	91.0	0.04	ESE
7	3.56	11.8	98.1	0.04	ESE
8	2.72	7.5	75.5	0.04	ENE
9	1.41	4.8	71.1	0.04	ENE
10	1.85	7.3	51.6	0.04	ENE

a length of 3–4 times the wavelength was applied. The simulation time was set to 1 h considering the time required for the stabilization of wave-induced currents. The significant wave height and the flow velocity and direction by layer for analyzing flow characteristics were output using 30-minute average values. SWASH version 7.01 was used for all numerical simulations, and numerical simulations were performed with 36 nodes in parallel using MPI (Message passing interface) to reduce the computation time.

4. Numerical Simulation Results

The results of previous studies indicate that the flow pattern in the hinterland of SBWs significantly varies depending on the installation location of SBWs, wave height, and wave direction. As such, input wave conditions were classified into ENE and ESE waves in this study, as described in section 2.2, with the flow simulation results of each case analyzed. Among the flow velocity simulation results by layer, the top layer adjacent to the sea level (near-surface layer, k1) and the bottom layer closest to the bottom (near-bottom layer, k4) were analyzed and indirectly compared with the topographic observation results because the simulation results of the near-surface layer (k1) can easily explain the flow pattern that occurs on the water surface while

the results of the near-bottom layer (k4) can easily describe the overall sediment transport pattern that occurs at the seabed of the coast. In this study, among the ten wave conditions for numerical simulation, two ENE and two ESE waves with high appearance rates and wave energy were calculated and the simulation results were analyzed (Table 4, Cases 1–4).

4.1 Significant Wave Height Results According to the Incident Wave Condition

When SBWs are installed as in Bongpo Beach, erosion and accretion at the opening and hinterland of the SBWs show different characteristics depending on the direction of the incident waves from the open sea, analyzed using the wave transformation simulation results of Bongpo Beach after introducing ENE and ESE waves are shown in Fig. 6, with areas with relatively high wave energy marked with red dotted lines. First, concerning ENE waves, a high significant wave height of more than 1.5 m reached the coastline through the openings of the SBWs (Fig. 6(a)), and the corresponding locations were eroded by more than 0.8 in the actual topographic observation. In the case of ESE waves, significant wave heights of approximately 2 m were introduced into the openings, and the entire hinterland of Cheonjin Port was particularly affected (Fig. 6(b)). Such wave energy

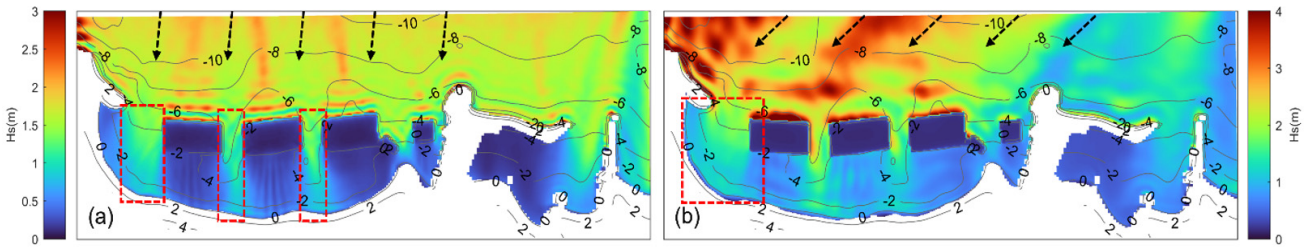


Fig. 6 Map view of calculated significant wave height H_s (colors) and areas with a H_s of 2 m or more (red dot line): (a) Wave condition of ENE series, (b) Wave condition of ESE series. The black arrows indicate the input wave direction.

distribution behind SBWs causes a rise in water level and the generation of diffracted waves in the hinterland, which is the main factor that develops cross-shore and longshore flows through the openings of SBWs.

4.2 Flow Simulation Results by Normal Incident Waves (ENE Series)

First, among the normal incident wave conditions, the flow patterns simulated in cases 1 and 2 with relatively high appearance rates and wave energy are shown in Fig. 7 and were analyzed. Figs. 7(a) to 7(b) show the simulation results at the near-surface layer (k1), while Figs. 7(c) to 7(d) show the simulation results at the near-bottom layer (k4). Overall, the flow patterns of both cases are not significantly different, and their magnitudes are somewhat different depending on the wave direction. The analysis of the flow velocity distribution shows that high flow velocity occurred near the coastline for both layers and that a large amount of sand was transported; in addition, topographic changes were caused in areas with a flow velocity of more than 0.4 m/s. For the flow of the k4 layer, 0.7 m/s or higher flows in the ESE

direction were generated near the coastline of the hinterland of the SBW openings where a large amount of wave energy was introduced, and the flow velocity in the hinterland of SBWs 2 and 3 decreased. These flow patterns were similar to the erosion and accretion patterns in sections 2 and 3, indicating that the flow was well reproduced. In section 1, as the erosion and accretion patterns were properly reproduced only in the hinterland of SBW 1, the section was divided again into sections 1-A and 1-B. In section 1-B area of the k1 layer, a strong flow (0.7 m/s or higher) was developed toward the hinterland of SBW 1 (S series) due to the strong incident wave energy through the opening between the Cheonjin Port breakwater and SBW 1 (Figs. 7 (a)–(b)), causing a strong flow (0.6 m/s or higher) toward the opening between SBWs 1 and 2 in the k4 layer (Figs. 7 (c)–(d)), effectively explaining the erosion and accretion patterns in section 1-B. However, in section 1-A, it is difficult to explain the erosion and accretion patterns in the opening between the Cheonjin Port breakwater and SBW with the simulated flow velocity patterns, indicating that ENE waves have limited influence on the sediment transport and topographic changes in section 1-A.

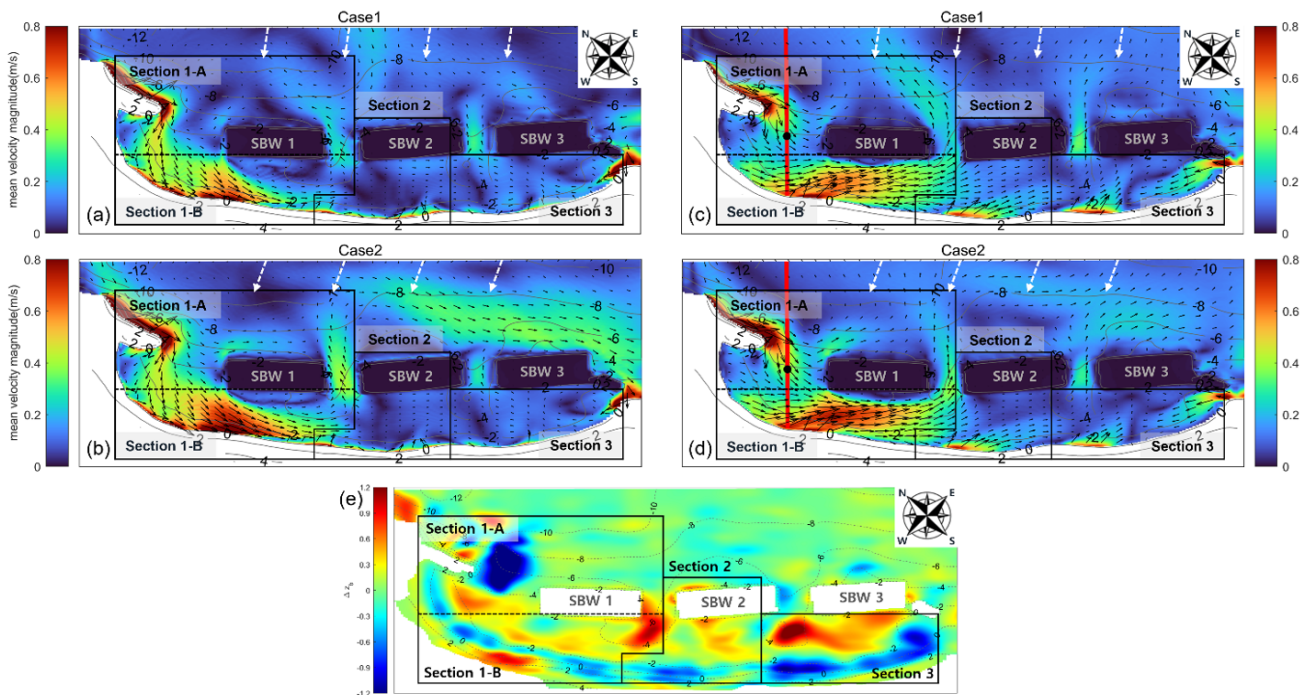


Fig. 7 Map view of simulated mean current velocity of (a) k1 in case1, (b) k1 in case2, (c) k4 in case1, (d) k4 in case2, and (e) Elevation difference (Δz_b) of measured bed level.

4.3 Flow Simulation Results by Oblique Incident Waves (ESE Series)

Among the ESE incident wave conditions, the numerical simulation results of cases 3 and 4 with relatively high wave energy and appearance rates are shown in Fig. 8. When ESE waves were introduced, the flow near the coastline was strongly developed in the near-surface layer (k1) and its magnitude was simulated to be more than 0.8 m/s (Figs. 8 (a)–(b)). In the case of the near-bottom layer (k4) that significantly affects sediment transport, it appears that the sediment transport of the coast was active when the flow velocity exceeded 0.4 m/s, which was particularly significant in section 1. This means that ESE waves caused sediment transport and topographic changes in section 1. A strong flow (0.6 m/s or higher) toward SBW 1 (SSE series) and a strong ES-series flow in the hinterland of SBW 1 (0.5 m/s or higher) occurred through the combination of the relatively

high wave energy introduced from the open sea, the reflected waves by the Cheonjin Port breakwater, and the refraction and diffraction of waves. These flows caused erosion in the corresponding areas and some of the lost sand was deposited in section 1-A with a relatively low flow velocity (0.1 m/s or less), consistent with the topographic observation results. This pattern is prominent in case 4 with relatively high wave energy (Fig. 8(d)).

Fig. 9 shows the flow velocity as red solid lines perpendicular to the coastline marked in Figs. 7(c) to 7(d) and Figs. 8(c) to 8(d). The flow velocity decreases in the opening between the Cheonjin Port breakwater and SBW 1, and that accretion is dominant in this area. The flow velocity variance was analyzed to be larger in Fig. 9(b) where ESE waves were simulated compared to Fig. 9(a) where ENE waves were introduced. This shows that ESE waves caused topographic changes more dominantly in section 1-A (opening between the

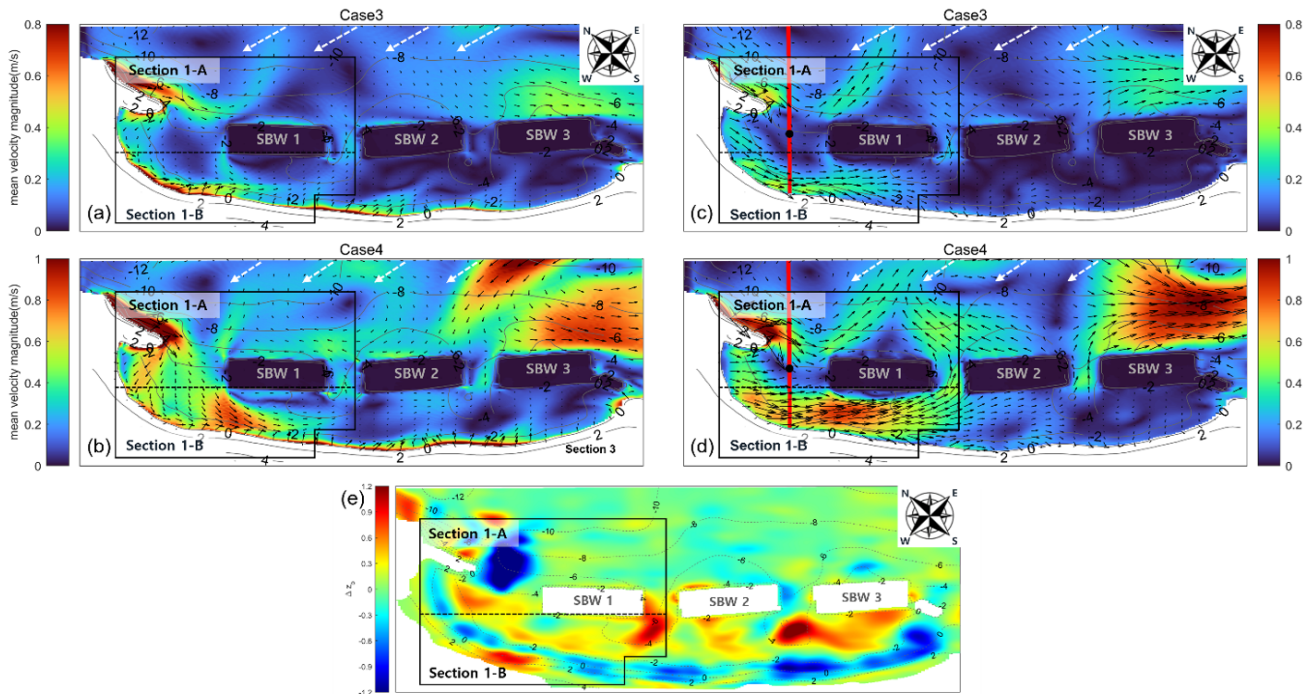


Fig. 8 Map view of simulated mean current velocity of (a) k1 in case3, (b) k1 in case4, (c) k4 in case3, (d) k4 in case4, and (e) Elevation difference (Δz_b) of measured bed level.

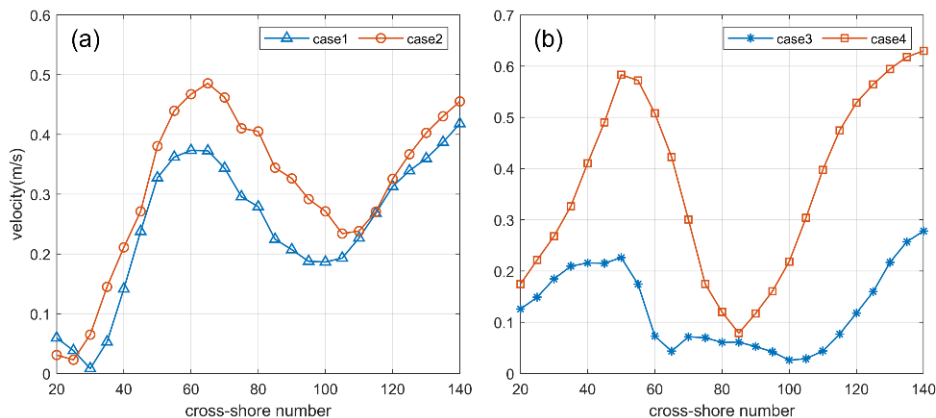


Fig. 9 Flow velocity variance of (a) ENE series and (b) ESE series between Cheonjin Port and SBW1.

Cheonjin Port breakwater and SBW 1) even though erosion and accretion were caused by both ENE and ESE waves.

5. Conclusions

In this study, numerical simulation was performed using field observation data to precisely analyze flow patterns that cause topographic changes and sediment transport in the coast where submerged breakwaters (SBWs) are installed, with the simulation results indirectly compared with topographic change observation data before and after a typhoon. Bongpo Beach, with SBWs installed through coastal maintenance projects tackling the continuous erosion problem, was selected as the study area. The wave and water depth data during the Typhoon Maysak period collected from Bongpo Beach were analyzed, revealing that both ENE waves, introduced in a direction perpendicular to the coastline, and ESE waves, introduced in oblique directions to the coastline, are dominant. In particular, it is considered that ESE waves caused sediment transport differently from large height swell-like waves in winter because they contain several high waves with a height of more than 3 m. Six water depth observations were performed from July 2020 to March 2021. Among them, the water depth data before and after Typhoon Maysak were compared and analyzed to examine the topographic changes in Bongpo Beach caused by storm waves (Fig. 3). The sand volume was calculated in places where the water depth difference was significant for effective analysis. Based on these calculations, Bongpo Beach was divided into three sections. The analysis results show that strong erosion occurred in areas close to the coastline of Bongpo Beach after the typhoon hit, similar to the characteristics of the 2-cell circulation pattern among the patterns presented in previous studies (Fig. 4(a)). However, there are limitations in understanding this phenomenon with observation data alone because structures other than the SBWs installed in Bongpo Beach, such as the Cheonjin Port breakwater and jetty, and various incident wave conditions transform the circulation patterns generated in the hinterland of the SBWs and create complex flows. To simulate such coastal flows, SWASH, a quasi-3D numerical model that can simulate vertical and horizontal flows simultaneously, was used. The simulation domain included all areas from Cheonjin Port to Bongpo Port, considering ESE waves introduced in oblique directions, and the grids of the area of interest with SBWs were more densely constructed using variable grids (curvilinear & non-equidistance grid) to improve the efficiency of numerical simulation. Four layers were divided in the vertical direction, with ten cases with different wave conditions created by applying the input reduction tool to the wave data obtained from acoustic waves and currents (AWAC). The simulation results showed that the direction of incident waves acted as a main factor that determines the flow pattern and topographic changes in Bongpo Beach where SBWs were installed and that the flows in the near-surface layer (k1) and near-bottom layer (k4) easily explain the overall sediment transport pattern in Bongpo Beach. When ENE waves were dominant, the flows toward the SBW hinterland in

the near-bottom layer (k4) were similar to the erosion and accretion patterns in sections 2 and 3. In section 1-B, the overall flows in the near-surface layer (k1) and near-bottom layer (k4) well explained the erosion and accretion patterns. In contrast, in section 1-A, when ESE waves were dominant, the strong flow near SBW 1 and the section with low flow velocity in the near-bottom layer (k4) were found to be similar to the erosion and accretion patterns. In particular, the analysis of the flow velocity variance shows that topographic changes in section 1-A were more dominantly caused by ESE waves than ENS waves.

These results indicate that it is possible to simulate the flow in Bongpo Beach where SBWs are installed by layer through the SWASH model and that the phenomena of sections where sediment transport and topographic changes are dominant can be inferred according to the incident wave conditions. This study failed to directly compare the numerical simulation results of flow by layer with the wave and flow velocity observation data during high wave occurrence periods, such as typhoons; however, the reliability of the model is considered high based on the results derived through an indirect comparison with the actual topographic change patterns. In addition, a comparison of the results of the quasi-3D model and the depth-averaged 2D model suggested that the quasi-3D model can predict the spatial flow pattern and sediment transport pattern in the hinterland of SBWs more accurately under high wave conditions, such as typhoons, which will be significantly helpful in designing efficient SBW arrangement plans.

Conflict of Interest

No potential conflict of interest relevant to this article was reported.

Funding

This study was partly supported by the National Research Foundation of Korea grant funded by the Korean government (NRF-2022 R111A3065599), and by the Korea CCUS Association (K-CCUS) grant funded by the Korean Government (KCCUS20220001, Human Resources Program for Reduction of greenhouse gases).

References

- da Silva, R. F., Hansen, J. E., Rijnsdorp, D. P., Lowe, R. J., & Buckley, M. L. (2022). The influence of submerged coastal structures on nearshore flows and wave runup. *Coastal Engineering*, 177 (August), 104194. <https://doi.org/10.1016/j.coastaleng.2022.104194>
- Dean, R. G., Chen, R., & Browder, A. E. (1997). Full scale monitoring study of a submerged breakwater, Palm Beach, Florida, USA. *Coastal Engineering*, 29(3-4), 291-315. [https://doi.org/10.1016/S0378-3839\(96\)00028-2](https://doi.org/10.1016/S0378-3839(96)00028-2)
- Deltares. (2017). *Input reduction tool – User manual*.

- Groenewoud, M. D., van de Graaff, J., Claessen, E. W. M., & van der Biezen, S. C. (1996). Effect of submerged breakwater on profile development. In *Coastal Engineering 1996*, 2428–2441. <https://doi.org/10.1061/9780784402429.188>
- Haller, M. C., Dalrymple, R. A., & Svendsen, I. A. (2002). Experimental study of nearshore dynamics on a barred beach with rip channels. *Journal of Geophysical Research*, 107(C6), 14-1-14-21. <https://doi.org/10.1029/2001jc000955>
- Jang, S., Cho, S., Park, W., & Jeong, H. (2014). A study on a characteristics of sediment transport around Myeongseondo at Jinha Beach. *Journal of Korean Society of Coastal Disaster Prevention*, 1(3), 118–125.
- Johnson, H. K., Karambas, T. V., Avgeris, I., Zanuttigh, B., Gonzalez-Marco, D., & Caceres, I. (2005). Modelling of waves and currents around submerged breakwaters. *Coastal Engineering*, 52(10–11), 949–969. <https://doi.org/10.1016/j.coastaleng.2005.09.011>
- Kang, M. H., Kim, J. S., Park, J. K., & Lee, J. S. (2015). Characteristics of wave-induced currents using the SWASH model in Haeundae Beach. *Journal of Korean Society of Coastal and Ocean Engineers*, 27(6), 382–390. <https://doi.org/10.9765/kscoe.2015.27.6.382>
- Korea Meteorological Administration (KMA). (2020). Open MET Data Portal. Retrieved from <https://data.kma.go.kr/cmmn/main.do>.
- Lee, J.-S., Park, M.-W., Kang, M.-H., & Kang, T.-S. (2015). Analysis of hydraulic characteristic in surf zone using the SWASH model during Typhoon NAKRI(1412) in Haeundae Beach. *Journal of the Korean Society of Marine Environment and Safety*, 21(5), 591–598. <https://doi.org/10.7837/kosomes.2015.21.5.591>
- Liang, B., Wu, G., Liu, F., Fan, H., & Li, H. (2015). Numerical study of wave transmission over double submerged breakwaters using non-hydrostatic wave model. *Oceanologia*, 57(4), 308–317. <https://doi.org/10.1016/j.oceano.2015.07.002>
- Lim, C., Kim, T. K., Lee, S., Yeon, Y. J., & Lee, J. L. (2021). Assessment of potential beach erosion risk and impact of coastal zone development: a case study on Bongpo-Cheonjin Beach. *Natural Hazards and Earth System Sciences*, 21(12), 3827–3842. <https://doi.org/10.5194/nhess-21-3827-2021>
- Lorenzoni, C., Postacchini, M., Mancinelli, A., & Brocchini, M. (2012). The morphological response of beaches protected by different breakwater configurations. *Coastal Engineering Proceedings*, 1(33), 52. <https://doi.org/10.9753/icce.v33.sediment.52>
- Magdalena, I., Atras, M. F., Sembiring, L., Nugroho, M. A., Labay, R. S. B., & Roque, M. P. (2020). Wave transmission by rectangular submerged breakwaters. *Computation*, 8(2), 56. <https://doi.org/10.3390/computation8020056>
- Marin, T. I., & Savov, B. (2017). Verification of the functional efficiency of submerged breakwaters by field measurements. *Coastal Engineering Proceedings*, 35, 18. <https://doi.org/10.9753/icce.v35.structures.18>
- Nobuoka, H., Irie, I., Kato, H., & Mimura, N. (1996). Regulation of Nearshore Circulation by Submerged Breakwater for Shore Protection. In *Coastal Engineering 1996*, 2391–2403. <https://doi.org/10.1061/9780784402429.185>
- Quataert, E., Storlazzi, C., van Dongeren, A., & McCall, R. (2020). The importance of explicitly modelling sea-swell waves for runup on reef-lined coasts. *Coastal Engineering*, 160, 103704. <https://doi.org/10.1016/j.coastaleng.2020.103704>
- Ranasinghe, R., Larson, M., & Savioli, J. (2010). Shoreline response to a single shore-parallel submerged breakwater. *Coastal Engineering*, 57(11–12), 1006–1017. <https://doi.org/10.1016/j.coastaleng.2010.06.002>
- Ranasinghe, R., & Turner, I. L. (2006). Shoreline response to submerged structures: A review. *Coastal Engineering*, 53(1), 65–79. <https://doi.org/10.1016/j.coastaleng.2005.08.003>
- Ranasinghe, R., Turner, I. L., & Symonds, G. (2006). Shoreline response to multi-functional artificial surfing reefs: A numerical and physical modelling study. *Coastal Engineering*, 53(7), 589–611. <https://doi.org/10.1016/j.coastaleng.2005.12.004>
- Rathnayaka, D., & Tajima, Y. (2020). Applicability of multilayer wave model for prediction of waves and undertow velocity profiles over a submerged breakwater. *Proceedings of the 10th International Conference on Asian and Pacific Coasts (APAC 2019)*, 76, 781–788. https://doi.org/10.1007/978-981-15-0291-0_107
- Smit, P., Zijlema, M., & Stelling, G. (2013). Depth-induced wave breaking in a non-hydrostatic, near-shore wave model. *Coastal Engineering*, 76, 1–16. <https://doi.org/10.1016/j.coastaleng.2013.01.008>
- Stelling, G. S., & Duijnmeijer, S. P. A. (2003). A staggered conservative scheme for every Froude number in rapidly varied shallow water flows. *International Journal for Numerical Methods in Fluids*, 43(12), 1329–1354. <https://doi.org/10.1002/flid.537>
- Stelling, G., & Zijlema, M. (2003). An accurate and efficient finite-difference algorithm for non-hydrostatic free-surface flow with application to wave propagation. *International Journal for Numerical Methods in Fluids*, 43(1), 1–23. <https://doi.org/10.1002/flid.595>
- Suzuki, T., Verwaest, T., & Hassan, W., Veale, W., Reyns, J., Trouw, K., Troch, P., & Zijlema, M. (2011). The applicability of SWASH model for wave transformation and wave overtopping: A case study for the Flemish coast. *Proceedings of the 5th International Conference on Advanced COmputational Methods in Engineering (ACOMEN 2011)*. <https://doi.org/10.13140/2.1.4232.7045>
- The SWASH team. (2020). SWASH user manual. *Simulating WAVes till SHore*, 1–152. https://swash.sourceforge.io/online_doc/swashuse/swashuse.html
- Villani, M., Bosboom, J., Zijlema, M., & Stive, M. J. . (2012). Circulation patterns and shoreline response induced by submerged breakwaters. *Coastal Engineering Proceedings*, 1(33), 25. <https://doi.org/10.9753/icce.v33.structures.25>
- Walmsley, T. V., Hanson, H., & Kraus, N. C. (2002). *Wave transmission at detached breakwaters for shoreline response modeling* [Technical note, CHETN-II-45]. <https://erdc-library.erdcren.dren>

mil/jspui/handle/11681/1913

Zijlema, M., & Stelling, G. S. (2008). Efficient computation of surf zone waves using the nonlinear shallow water equations with non-hydrostatic pressure. *Coastal Engineering*, 55(10), 780–790. <https://doi.org/10.1016/j.coastaleng.2008.02.020>

Zijlema, M., & Stelling, G. S. (2005). Further experiences with computing non-hydrostatic free-surface flows involving water waves. *International Journal for Numerical Methods in Fluids*, 48(2), 169–197. <https://doi.org/10.1002/flid.821>

Zijlema, M., Stelling, G., & Smit, P. (2011). SWASH: An operational public domain code for simulating wave fields and rapidly varied

flows in coastal waters. *Coastal Engineering*, 58(10), 992–1012. <https://doi.org/10.1016/j.coastaleng.2011.05.015>

Author ORCIDs

Author name	ORCID
Hwang, Yejin	0000-0002-5667-7630
Do, Kideok	0000-0001-7364-8375
Kim, Inho	0000-0003-3466-588X
Chang, Sungyeol	0000-0003-4641-4383

Instructions for Authors

General information

To submit a manuscript to the Journal of Ocean Engineering and Technology (JOET), it is advised to first carefully read the aims and the scope section of this journal, as it provides information on the editorial policy and the category of papers it accepts. Unlike many regular journals, JOET usually has no lag in acceptance of a manuscript and its publication. Authors that find a match with the aims and the scope of JOET are encouraged to submit as we publish works from all over the world. JOET adheres completely to guidelines and best practices published by professional organizations, including Principles of Transparency and Best Practice in Scholarly Publishing (joint statement by COPE, DOAJ, WAME, and OASPA (<http://doaj.org/bestpractice>) if otherwise not described below. As such, JOET would like to keep the principles and policies of those professional organizations during editing and the publication process.

Research and publication ethics

Details on publication ethics are found in <http://joet.org/authors/ethics.php>. For the policies on research and publication ethics not stated in the Instructions, Guidelines on Good Publication (<http://publicationethics.org/>) can be applied.

Requirement for membership

One of the authors who submits a paper or papers should be member of the Korean Society of Ocean Engineers (KSOE), except a case that editorial board provides special admission of submission.

Publication type

Article types include scholarly monographs (original research articles), technical articles (technical reports and data), and review articles. The paper should have not been submitted to other academic journal. When part or whole of a manuscript was already published to conference papers, research reports, and dissertations, then the corresponding author should note it clearly in the manuscript.

Copyright

After published to JOET, the copyright of manuscripts should belong to KSOE. A transfer of copyright (publishing agreement) form can be found in submission website (<http://www.joet.org>).

Manuscript submission

Manuscript should be submitted through the on-line submission website (<http://www.joet.org>). The date that manuscript was received through on-line website is the official date of receipt. Other correspondences can be sent by an email to the Editor in Chief or secretariat. The manuscript must be accompanied by a signed statement that it has been neither published nor currently submitted for publication elsewhere. The manuscript should be written in English or Korean. Ensure that online submission are in a standard word processing format. Corresponding author must write the manuscript using the JOET template provided in Hangul or MS Word format. Ensure that graphics are high-resolution.

Be sure all necessary files have been uploaded/ attached.

Authors' checklist

Please refer to "Authors' Checklist" for details.

Article structure

Manuscript must be edited in the following order: (1) Title, (2) Authors' names and affiliations, (3) Keywords, (4) Abstract, (5) Nomenclature (optional), (6) Introduction, (7) Main body (analyses, tests, results, and discussions), (8) Conclusions, (9) Conflict of interest, (10) Funding (optional), (11) Acknowledgements (optional), (12) References, (13) Appendices (optional), (14) Author's ORCIDs.

Abstract

A concise and factual abstract is required. The abstract should state briefly the background, purpose and methods of the research, the principal results and conclusions. An abstract should be written in 150-200 words. References are not cited in abstract whenever possible. Also, non-standard or uncommon abbreviations should be avoided, but if essential they must be defined at their first mention in the abstract itself.

Keywords

Immediately after the abstract, provide a maximum of 5 or 6 keywords.

Unit

Use the international system units(SI). If other units are mentioned, please give their equivalent in SI.

Equations

All mathematical equations should be clearly printed/typed using well accepted explanation. Superscripts and subscripts should be typed clearly above or below the base line. Equation numbers should be given in Arabic numerals enclosed in parentheses on the right-hand margin.

Tables

Tables should be numbered consecutively with Arabic numerals. Each table should be fully titled. All tables should be referred to in the texts.

Figures

Figures should be numbered consecutively with Arabic numerals. Each figure should be fully titled. All figures should be referred to in the texts. All the illustrations should be of high quality meeting with the publishing requirement with legible symbols and legends.

Conflict of interest

It should be disclosed here according to the statement in the Research and publication ethics regardless of existence of conflict of interest. If the authors have nothing to disclose, please state: "No potential

conflict of interest relevant to this article was reported.”

Funding

Funding to the research should be provided here. Providing a FundRef ID is recommended including the name of the funding agency, country and if available, the number of the grant provided by the funding agency. If the funding agency does not have a FundRef ID, please ask that agency to contact the FundRef registry (e-mail: fundref.registry@crossref.org). Additional detailed policy of FundRef description is available from <http://www.crossref.org/fundref/>. Example of a funding description is as follows: The study is supported by the Inha University research fund (FundRef ID: 10.13039/501100002632), and the Korea Health Personnel Licensing Examination Institute research fund (FundRef ID: 10.13039/501100003647).

Acknowledgments

Any persons that contributed to the study or the manuscript, but not meeting the requirements of an authorship could be placed here. For mentioning any persons or any organizations in this section, there should be a written permission from them.

References in text

References in texts follow the APA style. Authors can also see how references appear in manuscript text through the ‘Template’.

Reference list

Reference list follows the APA style. Authors can see how references should be given in reference section through the ‘Template’.

Appendices

The appendix is an optional section that can contain details and data supplemental to the main text. If there is more than an appendix, they should be identified as A, B, C, etc. Formulae and equations in appendices should be given separate numbering: Eq. (A1), Eq. (A2), etc.; in a subsequent appendix, Eq. (B1) and so on. Similarly for tables and figures: Table A1; Fig. A1, etc.

ORCID (Open Researcher and Contributor ID)

All authors are recommended to provide an ORCID. To obtain an ORCID, authors should register in the ORCID web site: <http://orcid.org>. Registration is free to every researcher in the world. Example of ORCID description is as follows:

Joonmo Chung: <https://orcid.org/0000-0003-1407-9031>

Peer review and publication process

The peer review process can be broadly summarized into three groups: author process, review process, and publishing process for accepted submissions. General scheme is presented in Figure 1.

Check-in process for review

If the manuscript does not fit the aims and scope of the Journal or does not adhere to the Instructions to Authors, it may be rejected immediately after receipt and without a review. Before reviewing, all submitted manuscripts are inspected by Similarity Check powered by iThenticate (<https://www.crossref.org/services/similarity-check/>), a plagiarism-screening tool. If a too high degree of similarity score is found, the Editorial Board will do a more profound content screening.

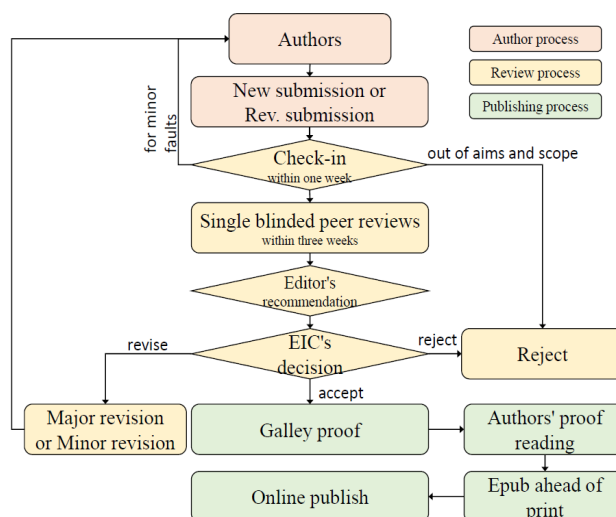


Figure 1 Flow chart of the peer review and publication process of JOET

The criterion for similarity rate for further screening is usually 15%; however, rather than the similarity rate, the Editorial Board focuses on cases where specific sentences or phrases are similar. The settings for Similarity Check screening are as follows: It excludes quotes, bibliography, small matches of 6 words, small sources of 1%, and the Methods section.

Number of reviewers

Reviewers will be selected from the list of reviewers. Manuscripts are then peer reviewed by at least 2 experts in the corresponding field, usually by 2.

Peer review process and the author response to the reviewer comments

JOET adopts single blind review, which means that the authors do not know the identity of the reviews. All papers, including those invited by the Editor, are subject to peer review.

The review period is 4 weeks. Usually the first decision is made within a week after completion of the review. The Editorial Board's decision after the review will be one of followings: Accept, Minor revision, Major revision, or Rejection. The Editorial Board may request the authors to revise the manuscript according to the reviewers' comments. If there are any requests for revision of the manuscript by the reviewers, the authors should do their best to revise the manuscript. If the reviewer's opinion is not acceptable or is believed to misinterpret the data, the author should reasonably indicate that. After revising the manuscript, the author should upload the revised files with a separate response sheet to each item of the reviewer's commentary. The author's revisions should be completed within 3 months after the request. If it is not received by the due date, the Editorial Board will notify the author. To extend the revision period beyond 3 months, the author should negotiate that with the Editorial Board. The manuscript review process can be provided for up two rounds. If the authors wish further review, the Editorial Board may consider it. The Editorial Board will make a final decision on the approval of the submitted manuscript for publication and can request any further corrections, revisions, and deletions of the article text if necessary. Statistical editing is also performed if the data requires professional statistical review by a statistician.

Processing after acceptance

If the manuscript is finally accepted, the galley proof will be sent to the corresponding author after professional manuscript editing and English proofreading. Proofreading should be performed for any misspellings or errors by the authors. Proofreading manuscript for publication is provided to the corresponding author, and the corresponding author must review the proofreading manuscript. Corresponding authors are responsible for the content of the proofreading manuscript and any errors. After final proofreading, the manuscript may appear at the journal homepage as an article in press with a unique DOI number for rapid communication. All published articles will be replaced by the replacement XML file and a final PDF.

Feedback after publication

If the authors or readers find any errors, or contents that should be revised, it can be requested from the Editorial Board. The Editorial Board may consider erratum, corrigendum or a retraction. If there are any revisions to the article, there will be a CrossMark description to announce the final draft. If there is a reader's opinion on the published article with the form of Letter to the editor, it will be forwarded to the authors. The authors can reply to the reader's letter. Letter to the editor and the author's reply may be also published.

How the journal handle complaints and appeals

The policy of JOET is primarily aimed at protecting the authors, reviewers, editors, and the publisher of the journal. If not described below, the process of handling complaints and appeals follows the guidelines of the Committee of Publication Ethics available from: <https://publicationethics.org/appeals>

- Who complains or makes an appeal?

Submitters, authors, reviewers, and readers may register complaints and appeals in a variety of cases as follows: falsification, fabrication, plagiarism, duplicate publication, authorship dispute, conflict of interest, ethical treatment of animals, informed consent, bias or unfair/inappropriate competitive acts, copyright, stolen data, defamation, and legal problem. If any individuals or institutions want to inform the cases, they can send a letter via the contact page on

our website: <https://www.joet.org/about/contact.php>. For the complaints or appeals, concrete data with answers to all factual questions (who, when, where, what, how, why) should be provided.

- Who is responsible to resolve and handle complaints and appeals?

The Editorial Board or Editorial Office is responsible for them. A legal consultant or ethics editor may be able to help with the decision making.

- What may be the consequence of remedy?

It depends on the type or degree of misconduct. The consequence of resolution will follow the guidelines of the Committee of Publication Ethics (COPE).

Article processing charge

Payment due

Article processing charge (APC) covers the range of publishing services JOET provides. This includes provision of online tools for editors and authors, article production and hosting, and customer services. Upon editorial acceptance of an article for the regular review service and upon submission of an article for the fast review service, the corresponding author will be notified that payment is due.

APC

The APC up to 6 pages is ₩300,000 (or \$300) and ₩650,000 (or \$650) for the for the regular and fast review services, respectively. An extra APC of \$100 per page is charged for papers longer than 6 pages. No taxes are included in this charge. For the fast review service, an advance fee of ₩250,000 (\$250) should be paid on submission.

Payment methods

Credit card payment can be made online using a secure payment form as soon as the manuscript has been editorially accepted. We will we send a receipt by email once payment has been processed. Please note that payment by credit card carries a surcharge of 10% of the total APC.

Invoice payment is due within 7 days of the manuscript receiving editorial acceptance. Receipts are available on request.

Title of Article

Firstname Lastname¹, Firstname Lastname² and Firstname Lastname³

¹Professor, Department of OO, OO School, OO University, Busan, Korea

²Graduate Student, Department of OO, OO University, Seoul, Korea

³Senior Researcher, Department of OO, OO Engineering, Corp., Seoul, Korea

KEYWORDS: Lumped mass line model, Explicit method, Steel lazy wave riser (Provide a maximum of 5 or 6 keywords.)

ABSTRACT:

****Abstract Construction Guidelines****

- 1) Describe the research background and aims in 1-2 sentences
- 2) Describe the research/analysis method (method section) in 2-3 sentences.
- 3) Describe the research/analysis results (results) in 2-3 sentences.
- 4) Describe the research conclusion in 1-2 sentences.

****Abstract Editing Guidelines****

- 1) Review English grammar.
- 2) Describe in 150-200 words.
- 3) When using an abbreviation or acronym, write the acronym after full words.
- 4) Abbreviations (acronyms) used only once should be written in full words only, and no acronyms.
- 5) References are not included in the abstract.

Nomenclature (Optional)

$ITOC$	Increment of total operating cost (\$/yr)
LHV	Lower heating value (kJ/kg)
P_w	Power (kW)
T	Temperature (K)
V	Volume (m ³)
ρ	Density (kg/m ³)

1. Introduction

The introduction should briefly place the study in a broad context and highlight why it is important. It should define the purpose of the work and its significance. The current state of the research field should be reviewed carefully and key publications cited. Please highlight controversial and diverging hypotheses when necessary. Finally, briefly mention the main aim of the work and highlight the principal conclusions. As far as possible, please keep the introduction comprehensible to scientists outside your particular field of research.

Received 00 February 2100, revised 00 October 2100, accepted 00 October 2100

Corresponding author Firstname Lastname: +82-51-759-0656, e-mail@e-mail.com

It is a recommended paper from the proceedings of 2019 spring symposium of the Korea Marine Robot Technology (KMRTS).

© 2100, The Korean Society of Ocean Engineers

This is an open access article distributed under the terms of the creative commons attribution non-commercial license (<http://creativecommons.org/licenses/by-nc/4.0>) which permits unrestricted non-commercial use, distribution, and reproduction in any medium, provided the original work is properly cited.

2. General Information for Authors

2.1 Research and Publication Ethics

Authorship should be limited to those who have made a significant contribution to the conception, design, execution, or interpretation of the reported study. All those who have made significant contributions should be listed as co-authors. Where there are others who have participated in certain substantive aspects of the research project, they should be acknowledged or listed as contributors.

The corresponding author should ensure that all appropriate co-authors and no inappropriate co-authors are included on the paper, and that all co-authors have seen and approved the final version of the paper and have agreed to its submission for publication.

Details on publication ethics are found in the journal's website (<http://joet.org/authors/ethics.php>). For the policies on research and publication ethics not stated in the Instructions, Guidelines on Good Publication (<http://publicationethics.org/>) can be applied.

2.2 Requirement for Membership

One of the authors who submits a paper or papers should be member of The Korea Society of Ocean Engineers (KSOE), except a case that editorial board provides special admission of submission.

2.3 Publication Type

Article types include scholarly monographs (original research articles), technical articles (technical reports and data), and review articles. The paper should have not been submitted to another academic journal. When part or whole of a manuscript was already published to conference papers, research reports, and dissertations, then the corresponding author should note it clearly in the manuscript.

Example: It is noted that this paper is revised edition based on proceedings of KAOST 2100 in Jeju.

2.4 Copyright

After published to JOET, the copyright of manuscripts should belong to KSOE. A transfer of copyright (publishing agreement) form can be found in submission website (<http://www.joet.org>).

2.5 Manuscript Submission

Manuscript should be submitted through the on-line submission website (<http://www.joet.org>). The date that manuscript was received through on-line website is the official date of receipt. Other correspondences can be sent by an email to the Editor in Chief or secretariat. The manuscript must be accompanied by a signed statement that it has been neither published nor currently submitted for publication elsewhere. The manuscript should be written in English or Korean. Ensure that online submission is in a standard word processing format. Corresponding author must write the manuscript using the JOET template provided in Hangul or MS Word format. Ensure that graphics are high-resolution. Be sure all necessary files have been uploaded/ attached.

2.5.1 Author's checklist

Author's checklist and Transfer of copyright can be found in submission homepage (<http://www.joet.org>).

3. Manuscript

Manuscript must be edited in the following order: (1) Title, (2) Authors' names and affiliations, (3) Keywords, (4) Abstract, (5) Nomenclature (optional), (6) Introduction, (7) Main body (analyses, tests, results, and discussions), (8) Conclusions, (9) Conflict of interest, (10) Funding (optional), (11) Acknowledgements (optional), (12) References, (13) Appendices (optional), (14) Author's ORCID's.

3.1 Unit

Use the international system units (SI). If other units are mentioned, please give their equivalent in SI.

3.2 Equations

All mathematical equations should be clearly printed/typed using well accepted explanation. Superscripts and subscripts should be typed clearly above or below the base line. Equation numbers should be given in Arabic numerals enclosed in parentheses on the right-hand margin. The parameters used in equation must be defined. They should be cited in the text as, for example, Eq. (1), or Eqs. (1)–(3).

$$G_{GEV}(x; \mu, \sigma, \xi) = \begin{cases} \exp[-(1 + \xi(x - \mu)/\sigma)^{-1/\xi}] & \xi \neq 0 \\ \exp[-\exp(-(x - \mu)/\sigma)] & \xi = 0 \end{cases} \quad (1)$$

in which μ , σ , and ξ represent the location (“Shift” in figures), scale, and shape parameters, respectively.

3.3 Tables

Tables should be numbered consecutively with Arabic numerals. Each table should be typed on a separate sheet of paper and be fully titled. All tables should be referred to in the texts.

Table 1 Tables should be placed in the main text near to the first time they are cited

Item	Buoyancy riser
Segment length ¹⁾ (m)	370
Outer diameter (m)	1.137
Inner diameter (m)	0.406
Dry weight (kg/m)	697
Bending rigidity (N·m ²)	1.66E8
Axial stiffness (N)	7.098E9
Inner flow density (kg·m ³)	881
Seabed stiffness (N/m/m ²)	6,000

¹⁾Tables may have a footer.

3.4 Figures

Figures should be numbered consecutively with Arabic numerals. Each figure should be fully titled. All the illustrations should be of high quality meeting with the publishing requirement with legible symbols and legends. All figures should be referred to in the texts. They should be referred to in the text as, for example, Fig. 1, or Figs. 1–3.

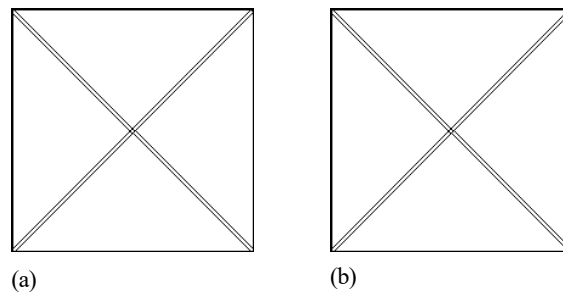


Fig. 1 Schemes follow the same formatting. If there are multiple panels, they should be listed as: (a) Description of what is contained in the first panel; (b) Description of what is contained in the second panel. Figures should be placed in the main text near to the first time they are cited

3.5 How to Describe the References in Main Texts

- JOET recommends to edit authors' references using MS-Word reference or ZOTERO plug-in
- How to add a new citation and source to a document using MS-Word is found in MS Office web page: <https://support.microsoft.com/en-us/office/add-citations-in-a-word-document-ab9322bb-a8d3-47f4-80c8-63c06779f127>
- How to add a new citation and source to a document using ZOTERO is found in zotero web page: <https://www.zotero.org/>

4. Results

This section may be divided by subheadings. It should provide a concise and precise description of the experimental results, their interpretation as well as the experimental conclusions that can be drawn. Tables and figures are recommended to present the results more rapidly and easily. Do not duplicate the content of a table or a figure with in the Results section. Briefly describe the core results related to the conclusion in the text when data are provided in tables or in figures. Supplementary results can be placed in the Appendix.

5. Discussion

Authors should discuss the results and how they can be interpreted in perspective of previous studies and of the working hypotheses. The findings and their implications should be discussed in the broadest context possible. Future research directions may also be highlighted

6. Conclusions

This section can be added to the manuscript.

Conflict of Interest

It should be disclosed here according to the statement in the Research and publication ethics regardless of existence of conflict of interest. If the authors have nothing to disclose, please state: “No potential conflict of interest relevant to this article was reported.”, “The authors declare no potential conflict of interest.”, “The authors declare that they have no conflict of interests.”

Funding (Optional)

Please add: “This research was funded by Name of Funder, grant number XXX” and “The OOO was funded by XXX”. Check carefully that the details given are accurate and use the standard spelling of funding agency names at <https://search.crossref.org/funding>

Acknowledgments (Optional)

In this section you can acknowledge any support given which is not covered by the author contribution or funding sections. This may include administrative and technical support, or donations in kind (e.g., materials used for experiments). For mentioning any persons or any organizations in this section, there should be a written permission from them.

References

JOET follows the American Psychological Association (APA) style.

- Some samples are found in following web pages: <https://apastyle.apa.org/style-grammar-guidelines/references/examples> or <https://www.ntnu.edu/viko/apa-examples>
- JOET recommends editing authors' references using MS-Word reference or ZOTERO plug-in
- How to add a new citation and source to a document using MS-Word is found in MS Office web page: <https://support.microsoft.com/en-us/office/add-citations-in-a-word-document-ab9322bb-a8d3-47f4-80c8-63c06779f127>
- How to add a new citation and source to a document using ZOTERO is found in ZOTERO web page: <https://www.zotero.org/>

Appendix (Optional)

The appendix is an optional section that can contain details and data supplemental to the main text. For example, explanations of experimental details that would disrupt the flow of the main text, but nonetheless remain crucial to understanding and reproducing the research shown; figures of replicates for experiments of which representative data is shown in the main text can be added here if brief, or as Supplementary data. Mathematical proofs of results not central to the paper can be added as an appendix.

All appendix sections must be cited in the main text. In the appendixes, Figures, Tables, etc. should be labeled starting with ‘A’, e.g., Fig. A1, Fig. A2, etc.

Examples:

<https://doi.org/10.26748/KSOE.2019.022>

<https://doi.org/10.26748/KSOE.2018.4.32.2.095>

Author ORCIDs

All authors are recommended to provide an ORCID. To obtain an ORCID, authors should register in the ORCID web site: <http://orcid.org>. Registration is free to every researcher in the world. Example of ORCID description is as follows:

Author name	ORCID
So, Hee	0000-0000-000-00X
Park, Hye-Il	0000-0000-000-00X
Yoo, All	0000-0000-000-00X
Jung, Jewerly	0000-0000-000-00X

Authors' Checklist

The following list will be useful during the final checking of a manuscript prior to sending it to the journal for review. Please submit this checklist to the KSOE when you submit your article.

< Checklist for manuscript preparation >

- I checked my manuscript has been 'spell-checked' and 'grammar-checked'.
- One author has been designated as the corresponding author with contact details such as
 - E-mail address
 - Phone numbers
- I checked abstract 1) stated briefly the purpose of the research, the principal results and major conclusions, 2) was written in 150–200 words, and 3) did not contain references (but if essential, then cite the author(s) and year(s)).
- I provided 5 or 6 keywords.
- I checked color figures were clearly marked as being intended for color reproduction on the Web and in print, or to be reproduced in color on the Web and in black-and-white in print.
- I checked all table and figure numbered consecutively in accordance with their appearance in the text.
- I checked abbreviations were defined at their first mention there and used with consistency throughout the article.
- I checked all references mentioned in the Reference list were cited in the text, and vice versa according to the APA style.
- I checked I used the international system units (SI) or SI-equivalent engineering units.

< Authorship checklist >

JOET considers individuals who meet all of the following criteria to be authors:

- Made a significant intellectual contribution to the theoretical development, system or experimental design, prototype development, and/or the analysis and interpretation of data associated with the work contained in the article.
- Contributed to drafting the article or reviewing and/or revising it for intellectual content.
- Approved the final version of the article as accepted for publication, including references.

< Checklist for publication ethics >

- I checked the work described has not been published previously (except in the form of an abstract or as a part of a published lecture or academic thesis).
- I checked when the work described has been published previously in other proceedings without copyright, it has clearly noted in the text.
- I checked permission has been obtained for use of copyrighted material from other sources including the Web.
- I have processed Plagiarism Prevention Check through reliable web sites such as www.kci.go.kr, <http://www.ithenticate.com/>, or <https://www.copykiller.org/> for my submission.
- I agree that final decision for my final manuscript can be changed according to results of Plagiarism Prevention Check by JOET administrator.
- I checked one author at least is member of the Korean Society of Ocean Engineers.
- I agreed all policies related to 'Research and Publication Ethics'
- I agreed to transfer copyright to the publisher as part of a journal publishing agreement and this article will not be published elsewhere including electronically in the same form, in English or in any other language, without the written consent of the copyright-holder.
- I made a payment for reviewing of the manuscript, and I will make a payment for publication on acceptance of the article.
- I have read and agree to the terms of Authors' Checklist.

Title of article :

Date of submission : DD/MM/YYYY

Corresponding author :

signature

Email address :

※ E-mail this with your signature to ksoehj@ksoc.or.kr

Publishing Agreement

ARTICLE DETAILS

Title of article :
Corresponding author :
E-mail address :
DOI : <https://doi.org/10.26748/KSOE.2XXX.XXX>

YOUR STATUS

I am one author signing on behalf of all co-authors of the manuscript.

ASSIGNMENT OF COPYRIGHT

I hereby assign to the Korean Society of Ocean Engineers, the copyright in the manuscript identified above and any tables, illustrations or other material submitted for publication as part of the manuscript (the "Article"). This assignment of rights means that I have granted to Korean Society of Ocean Engineers the exclusive right to publish and reproduce the Article, or any part of the Article, in print, electronic and all other media (whether now known or later developed), in any form, in all languages, throughout the world, for the full term of copyright, and the right to license others to do the same, effective when the Article is accepted for publication. This includes the right to enforce the rights granted hereunder against third parties.

SCHOLARLY COMMUNICATION RIGHTS

I understand that no rights in patents, trademarks or other intellectual property rights are transferred to the Journal owner. As the author of the Article, I understand that I shall have: (i) the same rights to reuse the Article as those allowed to third party users of the Article under the CC-BY-NC License, as well as (ii) the right to use the Article in a subsequent compilation of my works or to extend the Article to book length form, to include the Article in a thesis or

dissertation, or otherwise to use or re-use portions or excerpts in other works, for both commercial and non-commercial purposes. Except for such uses, I understand that the assignment of copyright to the Journal owner gives the Journal owner the exclusive right to make or sub-license commercial use.

USER RIGHTS

The publisher will apply the Creative Commons Attribution-Noncommercial Works 4.0 International License (CC-BY-NC) to the Article where it publishes the Article in the journal on its online platforms on an Open Access basis.

The CC-BY-NC license allows users to copy and distribute the Article, provided this is not done for commercial purposes and further does not permit distribution of the Article if it is changed or edited in any way, and provided the user gives appropriate credit (with a link to the formal publication through the relevant DOI), provides a link to the license, and that the licensor is not represented as endorsing the use made of the work. The full details of the license are available at <http://creativecommons.org/licenses/by-nc/4.0/legalcode>.

REVERSION OF RIGHTS

Articles may sometimes be accepted for publication but later rejected in the publication process, even in some cases after public posting in "Articles in Press" form, in which case all rights will revert to the author.

I have read and agree to the terms of the Journal Publishing Agreement.

Corresponding author:

name

signature

※ E-mail this with your signature to ksoehj@ksoe.or.kr (Papers will not be published unless this form is signed and returned)

Research and Publication Ethics

Journal of Ocean Engineering and Technology (JOET) adheres to the guidelines published by professional organizations, including Committee on Publication Ethics (COPE; <https://publicationethics.org/>)

1. Authorship

JOET considers individuals who meet all of the following criteria to be authors:

- 1) Made a significant intellectual contribution to the theoretical development, system or experimental design, prototype development, and/or the analysis and interpretation of data associated with the work contained in the article.
- 2) Contributed to drafting the article or reviewing and/or revising it for intellectual content.
- 3) Approved the final version of the article as accepted for publication, including references.

Contributors who do not meet all of the above criteria may be included in the Acknowledgment section of the article. Omitting an author who contributed to your article or including a person who did not fulfill all of the above requirements is considered a breach of publishing ethics.

Correction of authorship after publication: JOET does not correct authorship after publication unless a mistake has been made by the editorial staff.

2. Originality and Duplicate Publication

All submitted manuscripts should be original and should not be in consideration by other scientific journals for publication. Any part of the accepted manuscript should not be duplicated in any other scientific journal without permission of the Editorial Board, although the figures and tables can be used freely if the original source is verified according to the Creative Commons Attribution License (CC BY-NC). It is mandatory for all authors to resolve any copyright issues when citing a figure or table from other journal that is not open access.

3. Conflict-of-Interest Statement

Conflict of interest exists when an author or the author's institution, reviewer, or editor has financial or personal relationships that inappropriately influence or bias his or her actions. Such relationships are also known as dual commitments, competing interests, or competing loyalties. These relationships vary from being negligible to having a great potential for influencing judgment. Not all relationships represent true conflict of interest. On the other hand, the potential for conflict of interest can exist regardless of whether an individual believes that the relationship affects his or her scientific judgment. Financial relationships such as employment, consultancies, stock ownership, honoraria, and paid expert testimony are the most easily identifiable conflicts of interest and the most likely to undermine the credibility of the journal, the authors, or of the science itself. Conflicts can occur for other reasons as well, such as personal relationships, academic competition, and intellectual passion. If there are any conflicts of interest, authors should disclose them in the manuscript. The conflicts of interest may occur during the research process as well; however, it is important to provide disclosure. If there is a disclosure, editors, reviewers, and reader can approach the manuscript after understanding the situation and the background of the completed research.

4. Management Procedures for the Research and Publication Misconduct

When JOET faces suspected cases of research and publication misconduct such as a redundant (duplicate) publication, plagiarism, fabricated data, changes in authorship, undisclosed conflicts of interest, an ethical problem discovered with the submitted manuscript, a reviewer who has appropriated an author's idea or data, complaints against editors, and other issues, the resolving process will follow the flowchart provided by the Committee on Publication Ethics (<http://publicationethics.org/resources/flowcharts>). The Editorial Board of JOET will discuss the suspected cases and reach a decision. JOET will not hesitate to publish

errata, corrigenda, clarifications, retractions, and apologies when needed.

5. Editorial Responsibilities

The Editorial Board will continuously work to monitor and safeguard publication ethics: guidelines for retracting articles; maintenance of the integrity of the academic record; preclusion of business needs from compromising intellectual and ethical standards; publishing corrections, clarifications, retractions, and apologies when needed; and excluding plagiarism and fraudulent data. The editors maintain the following responsibilities: responsibility and authority to reject and accept articles; avoiding any conflict of interest with respect to articles they reject or accept; promoting publication of corrections or retractions when errors are found; and preservation of the anonymity of reviewers.

6. Hazards and human or animal subjects

If the work involves chemicals, procedures or equipment that have any unusual hazards inherent in their use, the author must clearly identify these in the manuscript. If the work involves the use of animal or human subjects, the author should ensure that the manuscript contains a statement that all procedures were performed in compliance with relevant laws and institutional guidelines and that the appropriate institutional committee(s) has approved them. Authors should include a statement in the manuscript that informed consent was obtained for experimentation with human subjects. The privacy rights of human subjects must always be observed.

Ensure correct use of the terms sex (when reporting biological factors) and gender (identity, psychosocial or cultural factors), and, unless inappropriate, report the sex and/or gender of study participants, the sex of animals or cells, and describe the methods used to determine sex and gender. If the study was done involving an exclusive population, for example in only one sex, authors should justify why, except in obvious cases. Authors should define how they determined race or ethnicity and justify their relevance.

7. Secondary publication

It is possible to republish manuscripts if the manuscripts satisfy the conditions of secondary publication. These are:

- The authors have received approval from the Editorial Board of both journals (the editor concerned with the secondary publication must have access to the primary version).
- The priority for the primary publication is respected by a publication interval negotiated by editors of both journals and the authors.
- The paper for secondary publication is intended for a different group of readers
- The secondary version faithfully reflects the data and interpretations of the primary version.
- The secondary version informs readers, peers, and documenting agencies that the paper has been published in whole or in part elsewhere, for example, with a note that might read, "This article is based on a study first reported in the [journal title, with full reference]"
- The title of the secondary publication should indicate that it is a secondary publication (complete or abridged republication or translation) of a primary publication.

8. Complaints and Appeals

The process of handling complaints and appeals follows the guidelines of the COPE available from: <https://publicationethics.org/appeals>

9. Post-publication discussions and corrections

The post-publication discussion is available through letter to editor. If any readers have a concern on any articles published, they can submit letter to editor on the articles. If there found any errors or mistakes in the article, it can be corrected through errata, corrigenda, or retraction.



The Korean Society of Ocean Engineers